Article

Not peer-reviewed version

Activated Carbon Ammonization: Effects of the Chemical Composition of the Starting Material and the Treatment Temperature

Silvia C. Oliveira , Romulo C Dutra , José J.L. León , Gesley A.V. Martins , Alysson M.A. Silva , Diana C.S. Azevedo , Rafeelle Gomes Santiago , Daniel Ballesteros Plata , Enrique Rodríguez-Castellón * , Marcos J Prauchner *

Posted Date: 8 January 2025

doi: 10.20944/preprints202501.0451.v1

Keywords: activated carbons; adsorption; surface chemistry; ammonization; N-doped carbons

 doi:10.20944/preprints202501.0451.v1

Article

Activated Carbon Ammonization: Effects of the Chemical Composition of the Starting Material and the Treatment Temperature

Silvia da C. Oliveira [1], Romulo C. Dutra [1], José J. L. León [1], Gesley A. V. Martins [1], Alysson M. A. Silva [2], Diana C. S. de Azevedo [3], Rafaelle G. Santiago [3], Daniel Ballesteros-Plata [4], Enrique Rodríguez-Castellón [4,*] and Marcos J Prauchner [1,*]

[1] Instituto de Química, Universidade de Brasília, Campus Darcy Ribeiro, Brasília/DF, CEP: 70904 970, Brazil
[2] Departamento de Engenharia Mecânica, Faculdade de Tecnologia, Universidade de Brasília, Campus Darcy Ribeiro, Brasília/DF, CEP: 70904 970, Brazil
[3] Departamento de Engenharia Química, Campus do Pici, bl. 731, Universidade Federal do Ceará, Fortaleza/CE, CEP: 60760-400, Brazil
[4] Departamento de Química Inorgánica, Cristalografía y Mineralogía, Instituto Interuniversitario de Investigación en Biorrefinerías I3B, Facultad de Ciencias, Universidad de Málaga, 29071 Málaga, Spain
* Correspondence: marcosjp@unb.br (M.J.P.); castellon@uma.es (E.R.-C.)

Abstract: N-containing carbon-based materials have been employed with claimed improved performance as adsorbent of acidic molecules, VOC and metallic ions, catalyst, electrocatalyst and supercapacitor. In this context, the present work provides valuable insights into the preparation of N-doped activated carbons (ACs) by thermal treatment in NH_3 atmosphere (ammonization). A commercial AC was submitted to two kinds of pre-treatment: (i) reflux with dilute HNO_3; (ii) thermal treatment up to 800 °C in inert atmosphere. The original and modified ACs were subjected to ammonization up to different temperatures. ACs with N content up to ~8% were achieved. Nevertheless, the amount and type of inserted nitrogen depended on ammonization temperature and surface composition of the starting material. Remarkably, oxygenated acidic groups on the surface of the starting material favored nitrogen insertion at low temperatures, with formation of mostly aliphatic (amines, imides, and lactams), pyridinic and pyrrolic nitrogens. In turn, high temperatures provoked the decomposition of labile aliphatic functions. Therefore, the AC prepared from the sample pre-treated with HNO_3, which had the highest content of oxygenated acidic groups among the materials submitted to ammonization, presented the highest N content after ammonization up to 400 °C, but the lowest content after ammonization up to 800 °C.

Keywords: activated carbons; adsorption; surface chemistry; ammonization; N-doped carbons

1. Introduction

Activated carbons (ACs) are non-toxic, inexpensive, and versatile materials that present pronounced porosity and therefore large specific surface area (SSA). This porosity usually comprises mainly micropores ($d < 2.0$ nm, where d is considered as the width of slit-shaped pores). However, considerable contents of mesopores ($2.0 \text{ nm} < d < 50$ nm) and macropores ($d > 50$ nm) can also be present.[1] Micropores contribute the most to SSA, while mesopores and macropores are usually more important as transport channels to improve the diffusion of substrates through the pore network towards the micropores, especially in liquid phase applications. Furthermore, narrow mesopores are responsible for the adsorption of large molecules that cannot access the micropores (e.g., dyes, pesticides, and toxins) [2–6].

Thanks to their well-developed and tunable porosity, ACs have been widely applied as adsorbents in gas separation, purification and storage, water and wastewater treatment, volatile

 doi:10.20944/preprints202501.0451.v1

recovery and removal of noxious substances from biological fluids, besides as drug carrier for controlled deliver [2–5,7–16]. Moreover, other properties, such as good electrical conductivity and high thermal, chemical and mechanical resistance make ACs very interesting materials to be used as catalyst, catalyst support, electrocatalyst and supercapacitor [6–8,16–20].

The arrangement of the carbon skeleton in ACs is complex and variable. However, in general terms, it can be envisaged that they are constituted by small segments of defective graphene layers containing something like five to seven rings. Some of these layers can stack together (not much more than 3 or 4 layers) to form such a kind of small graphitic microcrystals. These microdomains are bonded together in a continuous and random way, creating a stable network of carbon atoms. The empty spaces existing throughout the carbon structure correspond to the pores network [8].

Although sp^2 carbons are predominant, sp^3 or even sp carbons can also be found in ACs. Furthermore, hydrogen is present, mainly completing the valence of edge carbons. The H/C atomic ratio is usually taken as a measure of the aromaticity in carbon materials (the lower the ratio, the higher the aromaticity).

Other elements than carbon or hydrogen can also be present, mainly at the edges of the carbon layers. These other elements are called heteroatoms. Among them, oxygen is by far the most common, mainly because it is abundant in most of the usual AC precursors, especially in those derived from biomass, and part of this oxygen remains after the carbonization/activation process. Oxygen can be found in the form of several functional groups, as portrayed in Figure 1, which can be acidic (carboxylic acids, carboxylic anhydrides, lactones and phenols), nearly neutral (ether and ketones), or basic (as it is the case of quinones and pyrones) [21–25].

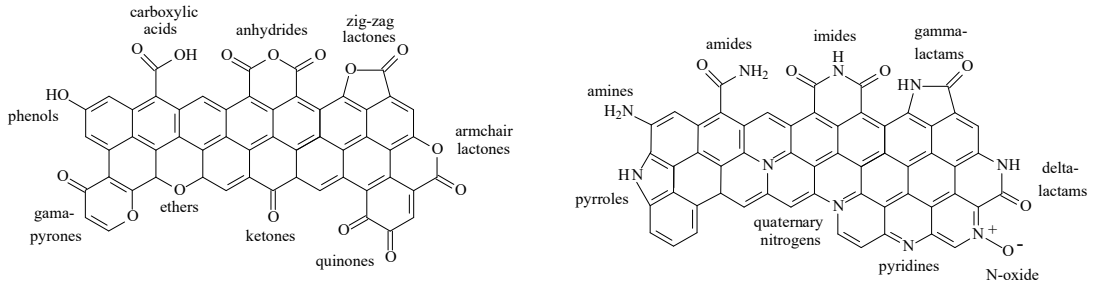

Figure 1. Usual oxygenated and nitrogenated functional groups present in ACs (elaborated considering references 21-27).

Another heteroatom that has aroused increasing interest is nitrogen, which can be found in the form of functional groups such as those displayed in Figure 1 [23–27]. Remarkably, the similar atomic radius between the elements facilitates the substitution of C by N in the carbon skeleton. Since nitrogen is relatively weakly electronegative (if compared to oxygen), the lone electrons pair on sp^3 nitrogen (Figure 2a) and pyridine (Figure 2b) is likely to interact with electrophilic entities. Furthermore, in some species, the lone electrons pair of N increases the density of π electrons on the basal plane of carbon and gives rise to a positive charge on the nitrogen atom, which enhances the material ability to interact with different species and to transfer electrons in redox reactions. This occurs when nitrogen contributes a pair of electrons for the π system, as are the cases of pyrrolic (Figure 2c) and quaternary (also called graphitic) nitrogens (Figure 2d), or even through resonance in aromatic amines (Figure 2e).

 doi:10.20944/preprints202501.0451.v1

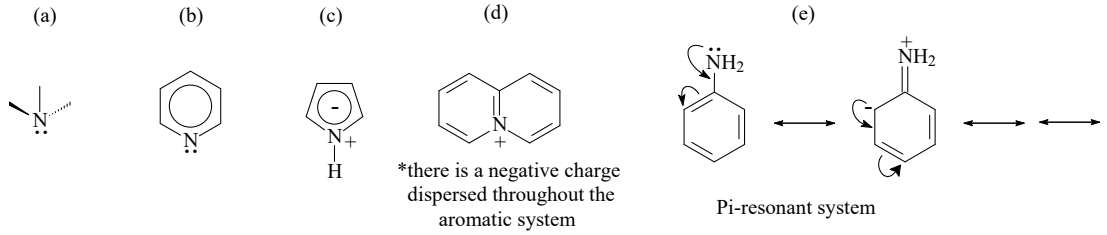

Figure 2. Illustration of the effect provoked by the pair of lone electrons of nitrogen in N-containing carbon-based materials.

Thanks to that, N-containing carbon-based materials (not only ACs but also carbon nanotubes, fullerenes, graphenes, carbon black, carbon foams, etc.) have been employed with claimed improved performance in several applications such as: adsorbent for the separation of acidic molecules such as CO_2 [27–43] and H_2S [44,45] from gaseous mixtures (i.e., biogas, natural gas, industrial exhaust gases and atmospheric air); adsorbent for the removal of metallic ions [14,46–51] and organic compounds [14,52] from water; catalyst or catalyst support [24,53–56]; metal-free electrocatalyst and photocatalyst for reactions such as O_2 [6,57–65], CO_2 [66–68] and hydrogen reduction [69,70]; supercapacitor [71–77]; electrode in metal-ion batteries [78–81], molecular sensors [82,83], and electromagnetic devices [84,8590]. AL-Hajri et al. [16] published a comprehensive review on recent applications of N-doped carbon materials in CO_2 capture and energy conversion and storage.

N-containing carbon-based materials can be prepared from natural precursors that have considerable content of this element. These are the cases of protein-rich biomasses such as bean dregs [46], yeast [53], chitosan [47], human hair [48], and leather waste [78], besides some synthetic polymers and resins [14,28–30,49,54,66,67,69]. Nevertheless, most of the raw materials widely employed for AC production (e.g., coal, coconut shell, wood, etc) are deficient in nitrogen. Thus, N-containing carbon-based materials can be obtained by mixing conventional N-deficient feedstocks with N-rich substrates such as melamine, urea and aniline [31–33,44,72]. Chemical vapor deposition (CVD) [57,82,86] and plasma processing [58] of N-rich substrates are less usual methodologies. Alternatively, nitrogen can be incorporated through a post-synthesis procedure, usually by heating a mixture of a carbon material with labile N-containing molecules such as urea and melanine [6,34,35,45,59–61,73,74,83,85], or by exposing a carbon material to a NH_3 atmosphere under heating (ammonization treatment, sometimes also called ammonification or amination) [26,36–40,50,52,55,62,68,75,76,87–90]. Finally, nitrogen molecules such as monoethanolamine and ethylendiamine, can be grafted on the surface of carbon-based materials [41,51,71]. The works of Kasera et al. [11], Rashidi et al. [41,77], Li et al. [42], Li et al. [56], Yuan et al. [81], Al-Hajri et al. [16], and Mainali et al. [91] provide comprehensive reviews on the synthesis of N-containing carbon-based materials.

Among the existing techniques to produce N-containing carbon-based materials, ammonization can be considered one of the most interesting (if not the most one) mainly because it imposes no restrictions as to the feedstock and activation methodology. However, there are currently few systematic studies correlating feedstock composition and experimental ammonization conditions with the composition and properties of the resulting materials. In this context, the present work aimed to provide new insights into the preparation of N-doped ACs and to conciliate these new insights with existing information dispersed throughout the literature. We therefore hope to contribute to increase the knowledge on this relevant subject and to improve the capacity to produce materials with surface properties tailored to specific needs. For that, a biomass-based commercial sample of a hierarchical micro-mesoporous AC (labelled herein WV) was subjected to ammonization up to 400 °C and 800 °C. These temperatures were chosen because, while 400 °C is a relatively low temperature that does not induce significant aromatization, 800 °C is high enough to do so. In addition, the original AC was also submitted to two types of pre-treatments: (i) with a HNO_3 solution (nitrification) to increase the material acidity and oxygen content; (ii) a thermal treatment up to 800

 doi:10.20944/preprints202501.0451.v1

°C in an inert atmosphere (complementary carbonization) to reduce the material acidity and oxygen content. Then, the modified ACs (obtained through complementary carbonization or nitrification) were also subjected to ammonization, so that the influence of the acidic oxygenated functional groups on nitrogen incorporation could be evaluated. The chemical composition of the materials was carefully evaluated through techniques such as X-ray photoelectron spectroscopy (XPS), temperature-programmed desorption coupled with mass spectrometry (TPD-MS), elemental analyses (EA) and Boehm titration, besides point of zero charge (PZC) measurements. Furthermore, the attaining of N_2 adsorption/desorption isotherms permitted to evaluate the textural properties.

2. Materials and Methods

2.1. Treatments

A commercial granular activated carbon (WV-A1050, supplied by MeadWestvaco—USA) was taken as starting material. According to the producer, the material was obtained from coconut shell (Cocos nucifera) by chemical activation with H_3PO_4. Before any treatment, the material (labelled herein as WV) was dried overnight at 110 °C and then cooled in desiccator with silica gel at room temperature. Figure 3 shows a scheme presenting the performed treatments and the labels attributed to the obtained samples.

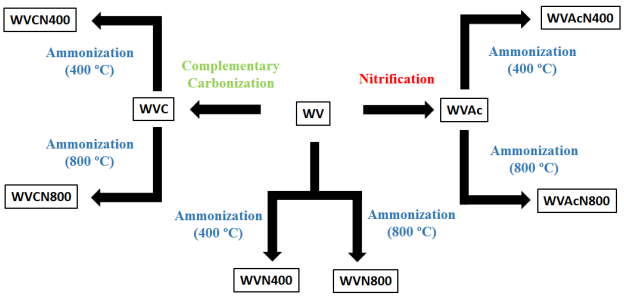

Figure 3. Scheme presenting the performed treatments and respective labels attributed to the obtained samples.

Nitrification was carried out by adding WV (20 g) to a beaker jar containing 200 mL of a 1.0 mol L^{-1} HNO_3 solution. The mixture was kept under reflux (~75 °C) and magnetic stirring for 1 h. After cooling, the material was washed with deionized water until the wash water reached a stable pH of ~6. After that, the obtained material, labelled as WVAc, was dried at 105 °C overnight.

Complementary carbonization and ammonization were carried out in a horizontal furnace equipped with a quartz tube. For carbonization, 8 g of WV were heated up to 800 °C (2 h; 5 °C min^{-1}) under inert atmosphere (N_2, 100 mL min^{-1}). The system was then left cool down to room temperature. The obtained material was labelled as WVC. For ammonization, 8 g of WV, WVC or WVAc were heated (5 °C min^{-1}) under NH_3 atmosphere (100 mL min^{-1}) to 400 (4 h) or 800 °C (1 h). The atmosphere was then switched to N_2 and the system was left cool down to room temperature. Initial exploratory tests were performed to select an adequate holding time at maximum temperature, that is to say, a time period that permits to achieve a nitrogen incorporation as high as possible without promoting excessive carbon etching. Based on these tests, 4 and 1 h were adopted as the holding times for ammonization up to 400 and 800 °C, respectively. The obtained samples were labelled as WVN400, WVCN400, WVAcN400, WVN800, WVCN800, and WVAcN800 according to the starting material and the maximum temperature used.

2.3. Materials Characterization

The textural characterization of the materials was based on N_2 adsorption/desorption isotherms acquired at -196 ºC using an Adsorption Analyzer model Autosorb IQ XR-XR Viton (Anton-Paar,

 doi:10.20944/preprints202501.0451.v1

USA). Samples were outgassed in situ under vacuum at 150°C for 8 h before analysis. The apparent SSA and the volume of micropores (V_{mic}) were determined by applying the Brunauer-Emmett-Teller (BET) and Dubinin-Radushkevich (DR) equations, respectively. The volume of liquid N_2 adsorbed at p/p_0 0.95, termed as $V_{0.95}$, was considered the volume of micro and mesopores (V_{mes}). Therefore, Vmes was determined by subtracting V_{mic} from $V_{0.95}$. The pore size distribution (PSD) curves were obtained using the software Autosorb 1 and applying the Quenched Solid Density Functional Theory (QSDFT) to the N_2 adsorption data.

The ash content was determined by heating the dried sample to 600 °C (6 h) under atmospheric air in an open muffle furnace. Ash composition was determined by Energy Dispersive X-ray Fluorescence spectroscopy (ED-XRF) using a Shimadzu equipment model EDS 720 HS.

C, H and N contents in the samples were measured on a Parkin Elmer CHN Elemental Analyzer model EA 2400 Series II equipped with an AD6 ultra-microbalance (Perkin Elmer).

The pH value at which the net charge on a surface is zero is termed the point of zero charge (PZC). It was determined based on an approach widely described in the literature (see, just as an example, reference [92]). Eleven solutions with pH (initial pH, pHi) varying in the range from 2 to 12 were prepared by taking 20 mL of 0.100 mol L^{-1} NaCl (background electrolyte) and adjusting the pH with 0.100 mol L^{-1} NaOH or HCl solutions. 20.0 mg of AC were added to each solution and the flasks were shaken for 24 h at room temperature. The pH of the resulting supernatant liquid (final pH, pHf) was measured and the difference between pHi and pHf was plotted against pHi. PZC was identified as the pHi value corresponding to the point where the curve crossed the abscissa axis.

TPD-MS analyses were performed on an automated reaction system model AMI-90R from Altamira Instruments (USA) coupled to a Dymaxion quadrupole mass spectrometer (range 0–100 m/z). The sample (ca. 100.0 mg) was placed in a quartz U-tube under an Ar flow of 10 cm^3 min^{-1} and atmospheric pressure, and then heated to 100 °C (10 °C min^{-1}) and maintained at this temperature for 60 min to remove water and other adsorbed small molecules. The temperature was then raised to 950 °C using the same heating rate. The evolved gases were continuously monitored with the mass spectrometer. CO and CO_2-profiles were fitted assuming Gaussian distribution for each peak. Peaks areas were correlated to the amount of gas through a daily routine calibration that consisted in the injection of a known volume of pure gas using a calibrated loop [23].

The contents of acid and basic groups were determined using a procedure based on the Boehm's titration method [93]. Shortly, the basic content was determined by adding 0.50 g of AC to an Erlenmeyer flask containing 50 mL of a standard HCl solution (~0.100 mol L^{-1}). After magnetic stirring for 24 h and filtration, aliquots of 10 mL of the filtrate were titrated against a standard NaOH solution ~0.100 mol L^{-1}. In turn, the content of acidic groups was determined by backtitration: about 0.50 g of AC was added to an Erlenmeyer flask containing 50 mL of the standard NaOH solution. After magnetic stirring for 24 h and filtration, 10 mL aliquots of the filtrate were added to 15 mL of the standard HCl solution. Finally, the excess acid was titrated with the standard NaOH solution. Blank tests were performed following the same methodology, but without the addition of AC. Thus, the contents of acidic or basic groups were determined taking into account the difference between the volumes of NaOH solution spent to reach the endpoint in the titrations of the sample and the blank. Measurements were taken in triplicate.

XPS measurements were carried out using a Physical Electronics 5700 spectrometer using the Mg-Kα line (1253.6 eV) from a PHI model 04-548 Dual Anode X-rays Source. The X-rays source was run at a power of 300 W (10 keV and 30 mA). The pressure inside the vacuum chamber was 5×10^{-7} Pa. A hemispherical analyzer was employed (10-360 Precision Energy Analyzer) with a multi-channel detector. The specimens were analyzed at an angle of 45° to the surface plane. Binding energies (BE) were referred to the C1*s* line of adventitious carbon at 284.8 eV and determined with the resolution of ±0.1 eV. The spectra were fitted assuming Gaussian-Lorentzian distribution for each peak.

 doi:10.20944/preprints202501.0451.v1

3. Results

3.1. Characterization of the Unmodified AC WV

The N_2 adsorption-desorption isotherms of the unmodified AC WV are displayed in Figure 4a. According to IUPAC classification [1], the adsorption branch can be classified as a hybrid of types I(b) and IV isotherms, which are typical for microporous and mesoporous materials, respectively. This is in accordance with the textural properties compiled in Table 1, where the volumes of micro and mesopores for WV were 0.50 and 0.42 $cm^3\ g^{-1}$, respectively, with a high SSA of 1508 $m^2\ g^{-1}$. The presence of mesopores is confirmed by the occurrence of a prominent hysteresis loop above p/p_0 ~0.4. This hysteresis loop resembles H4-type, which is associated with slit-shaped pores [1].

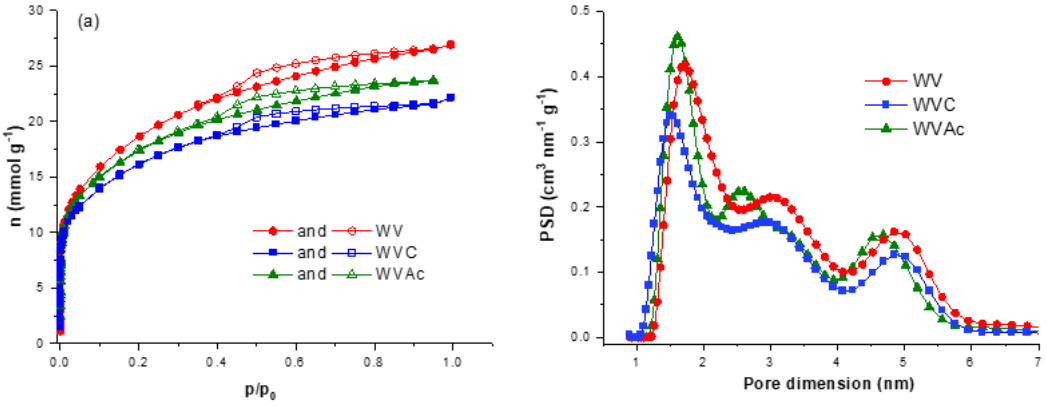

Figure 4. (a) N_2 adsorption-desorption isotherms and (b) corresponding PSD curves (closed and open symbols correspond to the adsorption and desorption branches, respectively).

Table 1. Data of textural characterization.

Sample	S_{BET} ($m^2\ g^{-1}$)	V_{mic} ($cm^3\ g^{-1}$)	$V_{0.95}$ ($cm^3\ g^{-1}$)	V_{mes} ($cm^3\ g^{-1}$)
WV	1506	0.51	0.92	0.41
WVN400	1238	0.39	0.72	0.33
WVN800	1247	0.42	0.74	0.32
WVC	1296	0.44	0.75	0.31
WVCN400	1289	0.43	0.74	0.31
WVCN800	1313	0.46	0.76	0.30
WVAc	1392	0.47	0.82	0.35
WVAcN400	1226	0.41	0.72	0.31
WVAcN800	1504	0.50	0.83	0.33

WV presented a relatively high ash content, 4.2 wt%. The ash was analyzed by ED-XRF, which permitted the identification of the following elements and their respective weight percentages (relative to the mass of the dry WV before burning): P 1.2; Na 0.7; Si 0.1; Ca 0.1 (only elements with weight percentage ≥ 0.1 were listed here). The presence of some phosphorus is due to the chemical activating agent (H_3PO_4) [35,51,71,94–96], while the metallic elements must be remnants of the biomass precursor composition.

The results of elemental analysis (Table 2) showed that WV has a relatively high H/C atomic ratio of 0.41, which indicates a low aromaticity degree. Furthermore, the sum of C, H, N and ash contents amounted to only 87.1 wt%, which evidence that the sample has a high O content. These findings are consistent with the fact that chemical activation with H_3PO_4 is usually carried out up to relatively low temperatures (in the range of 400-550 °C) [35,51,71,94,97] at which the carbonization

 doi:10.20944/preprints202501.0451.v1

process is still at an early stage. Finally, it is worth to highlight that the N content was quite low, 0.2 wt%.

Table 2. Data of mass variation during ammonization (Δm_{am}), PZC, elemental analyses and titration.

Sample	[1]Δm_{am} (%)	PZC	Elemental analysis				Titration (mmol g^{-1})	
			C (wt%)	H (wt%)	N (wt%)	[2]H/C	Acidic	Basic
WV	-	4.7	80.0	2.7	0.2	0.41	1.11	0.45
WVN400	-4.2	6.8	73	2.4	3.9	0.39	0.50	0.38
WVN800	-10.8	6.2	79.0	1.9	5.5	0.29	0.33	0.75
WVC	-	6.2	84.9	1.1	0.2	0.16	0.19	0.32
WVCN400	+3.2	6.1	78.2	1.0	2.8	0.15	0.15	0.43
WVCN800	-1.5	6.3	82.5	1.3	3.5	0.19	0.07	0.86
WVAc	-	1.8	80.2	3.2	2.7	0.48	1.94	0.00
WVAcN400	-1.8	3.4	77.4	3.2	6.8	0.50	1.06	0.64
WVAcN800	-32.4	6.9	89.9	1.4	1.6	0.19	0.32	0.68

[1] Mass variation during ammonization. [2] Atomic ratio.

The survey XPS spectrum of WV is displayed in Figure S2a (SI). The elemental composition (wt%) determined from the high resolution (HR) XPS spectra was: C 83.1; O 13.7; N 0.3; P 1.3; Na 1.3; Si 0.3 (Table 3). It is worth to point out that the data regarding phosphorous and metallic elements are in good accordance with the above reported ED-XRF data obtained from ashes analyses. In turn, the C and N contents are relatively well in agreement with the data of elemental analysis (Table 2). Taking into account that XPS is a superficial technique that provides an estimation of the chemical composition of the few uppermost layers of the external surface, while elemental analysis and ash analysis by ED-XRF scrutinize the composition of the material as a bulk, thus it is possible to conclude that WV has a fairly homogeneous chemical composition through the radial direction.

Table 3. Data of surface chemical composition determined by XPS.

Sample	Element content (wt%)					
	C	O	N	P	Na	Si
WV	83.1	13.7	0.3	1.3	1.3	0.3
WVN400	83.2	10.7	3.1	1.3	1.2	0.5
WVN800	84.9	7.2	5.1	1.2	1.0	0.6
WVC	86.2	8.4	0.8	2.4	1.6	0.6
WVCN400	85.3	8.1	3.1	1.8	0.7	1.0
WVCN800	85.3	7.6	3.9	1.1	1.1	1.1
WVAc	80.1	17.0	1.7	0.8	-	0.4
WVAcN400	81.4	9.5	7.8	1.0	-	0.3
WVAcN800	89.1	8.3	1.9	0.4	-	0.3

The HR C 1*s* core level spectrum of WV was deconvoluted into four components (Figure 5a), which were assigned, in accordance with the literature [98], mainly to: unfunctionalized carbons, mostly aromatic carbons (CI peak; 284.8 eV); C–O (CII peak; 286.2 eV); C=O (CIII peak; 287.4 eV); COO^- (CIV peak; 288.8 eV). The relative contributions of each peak are reported in Table 4.

 doi:10.20944/preprints202501.0451.v1

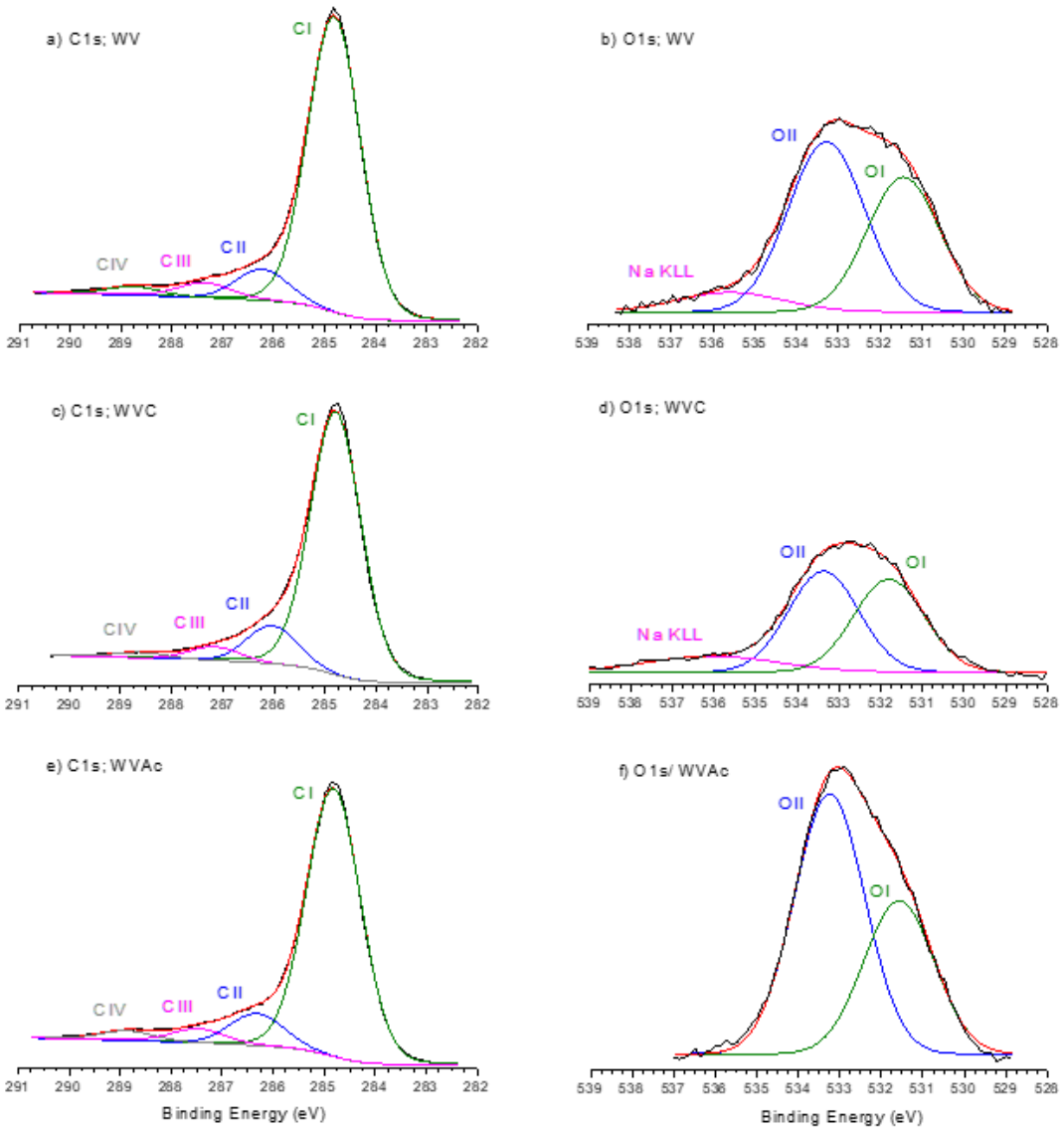

Figure 5. HR XPS C 1*s* and O 1*s* spectra.

Concerning the deconvolution of the HR O1*s* core level spectrum of ACs and the assignment of the resulting peaks, the literature brings plenty of conflicting information. The website corresponding to reference [99] displays a compilation of data concerning the assignment of O 1*s* peaks for a variety of O-containing functionalities, which were taken from the work of Beamson and Briggs [100]. These data were used to elaborate Figure S1 in Supplementary Information (SI). This Figure makes clear that, independent of the functional group, O double bounded to C tends to yield O 1*s* peaks at lower BEs, in the range of around 531-533 eV, while oxygen single bounded to carbon tends to render O1*s* peaks at higher Bes, in the range of around 533-534 eV. Therefore, a simplified procedure was adopted in the present work, which consisted in deconvoluting the O1*s* envelope into only two peaks assigned to oxygen in C=O (OI peak) and C–O (OII peak) moieties. This procedure has been largely adopted by several authors [49,51,61,67,96] because it is able to provide relevant information while avoids doubtful interpretations. Furthermore, it is in accordance with the work of Smith et al. [101], which employed DFT calculations and experimental data to deconvolute and assign the O 1s peaks of model compounds.

 doi:10.20944/preprints202501.0451.v1

Table 4. Relative contributions of C 1*s* and O 1*s* peaks obtained from the HR XPS spectra considering each element separately and, between brackets, all the identified elements.

Sample	Relative contributions (wt%)					
	CI	CII	CIII	CIV	OI	OII
WV	83.7 (69.5)	8.7 (7.2)	4.9 (4.1)	2.7 (2.2)	42.9 (5.8)	57.1 (7.8)
WVN400	82.7 (68.7)	11.3 (9.4)	3.9 (3.3)	2.1 (1.7)	57.5 (6.2)	42.5 (4.6)
WVN800	79.3 (67.3)	13.8 (11.8)	4.8 (4.1)	2.1 (1.8)	46.3 (3.7)	53.7 (3.5)
WVC	82.8 (71.4)	11.4 (9.8)	4.1 (3.5)	1.7 (1.5)	47.9 (4.0)	52.1 (4.3)
WVCN400	80.8 (68.9)	12.6 (10.7)	4.8 (4.1)	1.8 (1.6)	48.1 (3.9)	51.9 (4.2)
WVCN800	79.8 (68.1)	13.0 (11.1)	5.0 (4.3)	2.2 (1.8)	46.4 (3.5)	53.6 (4.1)
WVAc	82.2 (65.8)	9.7 (7.8)	4.9 (3.9)	3.2 (2.6)	37.0 (6.3)	63.0 (10.7)
WVAcN400	76.3 (62.1)	14.8 (12.0)	6.2 (5.1)	2.7 (2.2)	53.1 (5.0)	46.9 (4.4)
WVAcN800	76.4 (68.0)	15.1 (13.4)	6.4 (5.7)	2.1 (1.9)	10.8 (0.9)	89.2 (7.4)

At this point, it is worth to mention that, for the samples that contain small amounts of Na, a KLL Auger signal of this element was identified (Table 3) at around 535.6 eV. Since this signal partially overlapped the O 1*s* envelope, it was separated from OI and OII peaks during deconvolution. By doing that, the O 1*s* XPS spectrum of WV gave rise to OI and OII peaks centered at 531.4 and 533.3 eV, respectively (Figure 5b; Table 4).

The deconvolution of the HR P 2*p* core level spectra and the assignment of the resulting peaks are also difficult for this kind of material. The oxidation state of P atoms can vary from lower values in C_3P like groups, which give rise to P 2*p* peaks in the range of 130-131 eV, up to higher values in $P(=O)(-O)_3$ like groups, which give rise to peaks at higher BEs (around 134 eV) [71,74,100–102]. In the case of WV, the P 2*p* envelope was located mostly between 132 and 134 eV (Figure 6), which indicates the presence of groups containing a P atom bonded to one or more O atoms: $C_3P(=O)$, $C_2P(=O)(-O)$, $CP(=O)(-O)_2$ and $P(=O)(-O)_3$ like groups.

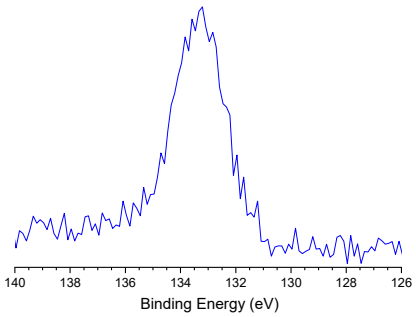

Figure 6. HR P 2*p* core level spectrum for the unmodified AC WV.

In accordance with its high O content and low aromaticity, WV rendered relatively intense CO_2, CO, H_2O and H_2 emissions during TPD analysis (Figure 7). CO and CO_2-TPD profiles have been widely employed to identify oxygenated functionalities on the surface of carbon-based materials. However, the peak assignment is not such a trivial task and there is contradictory information in the literature, as clearly evidenced by the data compiled by Figueiredo et al. [22] and Herold et al. [102]. This occurs mainly because, as a general rule, many different oxygenated functional groups that release CO_2, CO or both coexist and can be found inserted in a large variety of chemical environments. In this way, the decomposition temperature of a given group can vary throughout a relatively large temperature range and the occurrence of overlapping peaks is quite usual.

 doi:10.20944/preprints202501.0451.v1

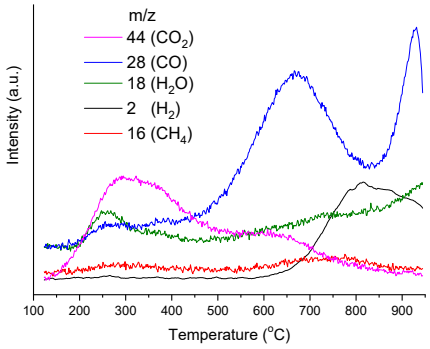

Figure 7. TPD profiles for the unmodified AC WV.

In the present work, the CO_2-TPD profile of WV was deconvoluted into five peaks (Figure 8a) whose assignments were done according to references [23,103–106]. In this sense, the first two peaks (CO_2-I at 278 °C and CO_2-II at 388 °C) were assigned to the decomposition of stronger and weaker carboxylic acids, respectively. The third peak (CO_2-III at 518 °C) was assigned to carboxylic anhydrides. In turn, the last two peaks (CO_2-IV at 640 °C and CO_2-V at 765 °C) were mainly assigned to lactones (although it is worth to mention that they can have some contribution from the conversion of CO into CO_2, as it will be opportunely discussed in Subsection 3.4.1).

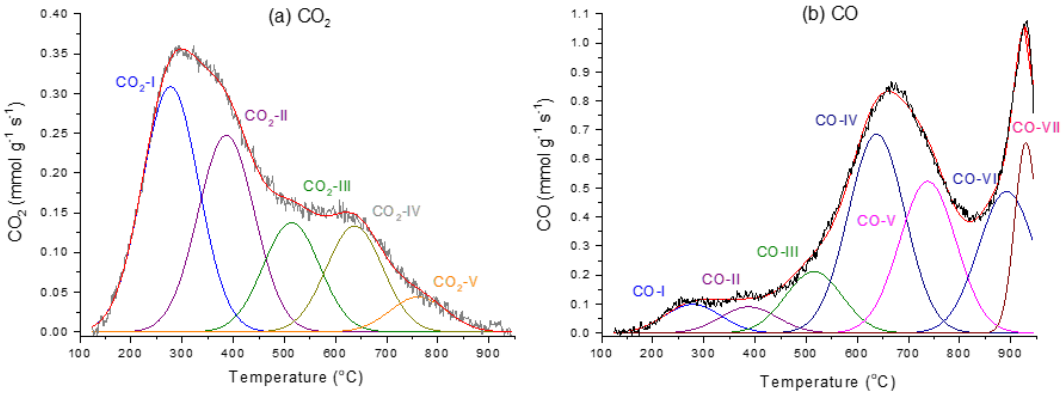

Figure 8. (a) CO_2 and (b) CO-TPD profiles of WV and respective deconvoluted peaks.

In turn, the CO-TPD profile was deconvoluted into seven peaks (Figure 8b). The first two (CO-I at 278 °C and CO-II at 388 °C) also correspond to the decomposition of carboxylic acids. Although the decomposition of these groups did not release CO by itself, the fragmentation of CO_2^+ ions in the ionization chamber of the mass spectrometer generates CO^+ ions [23]. Furthermore, the possibility that CO was also formed inside the sample cell itself due to the conversion of as-formed CO_2 molecules catalyzed by the AC surface (Boudouard reaction [107]) cannot be ruled out. The third CO peak (CO-III at 515 °C) was assigned to carboxylic anhydrides, which release both CO_2 and CO simultaneously (therefore, the CO-III and CO_2-III peaks were located at almost the same temperature).

Before proceeding with the assignments for the other CO peaks, it is worth to highlight that, while on the one hand there is agreement that the presence of an intense CO emission peak in the ~600-700 °C range is due to the decomposition of phenols/ethers [23,103–106,108], on the other hand there are controversial proposals for the assignment concerning to CO emission in the ~700-800 °C range. For example, Rocha et al. [23] and Li et al. [103] attributed this emission to carbonyl groups in ketone and quinone-like structures. However, Ishii and Ozaki [105], who carried out a detailed work involving TPD analyses of ACs isotopically labeled with deuterium, attributed both the CO peaks observed at 636 and 750 °C to decomposition of phenol/ether groups, while the emissions due to the

 doi:10.20944/preprints202501.0451.v1

decomposition of carbonyl-containing functionalities were assigned to peaks at higher temperatures. In addition, Düngen et al. [108], who achieved a better peak separation by carrying out non-linear TPD analyses of carbon-based material, concluded that, while phenols and ethers decompose between 620 and 800 °C, carbonyl-containing functions decompose all only above 800 °C.

In the present work, the assignments of the CO peaks were made according to the proposal of the Ishii and Düngen teams. Thus, the peaks verified at 648 and 737 °C (CO-IV and CO-V peaks) in the CO-TPD profile of WV were both assigned to C─O─H/C moieties in phenols/ethers, while the peaks at around 892 and 930 °C (CO-VI and CO-VII) were assigned to carbonyl-containing groups (ketones/quinones). The adoption of this assignment line was supported by the fact that, as will be reported in Subsection 3.3, the intensity of the CO-V peak increased after nitrification of WV, whereas the peaks above around 800 °C vanished. Therefore, if it is assumed that the treatment with HNO_3 increases the amount of phenolic groups and oxidizes existing carbonyl groups, then it is possible to infer that the CO-V peak was due to C─O─H/C motifs in phenols/ethers, while the CO-VI and CO-VII peaks were due to carbonyl-containing groups.

In accordance with TPD analyses, the titration of WV resulted in a relatively high content of acidic groups, 1.11 mmol g^{-1}, besides a moderate content of basic groups, 0.45 mmol g^{-1} (Table 2). Accordingly, WV presented a somewhat acidic PZC of 4.7.

3.2. Complementary Carbonization of WV

As already mentioned in the previous Subsection, chemical activation with H_3PO4 is usually carried out up to relatively low temperatures (usually 400-550 °C) and, therefore, the resulting materials are still in an incipient carbonization degree. Therefore, to achieve a material with higher aromaticity and lower content of acidic oxygenated functional groups, WV was submitted to a complementary carbonization up to 800 °C.

As expected, the complementary carbonization of WV gave rise to a considerable weight loss, 12.4 wt%. Since a TPD experiment can be considered as a kind of carbonization in small scale, the reasons for the quoted weight loss can be disclosed taking into account the TPD profiles of WV. In this sense, the majority of the weight loss can be attributed to the release of CO_2 and CO due to the decomposition of oxygenated groups (Figures 7 and 8; see pertinent discussions in Subsection 3.1). Furthermore, the releases of H_2O, H_2 and CH_4 (Figure 7) have minor contributions. The release of H_2O in the range of ~200-320 °C is mainly attributed to the occurrence of dehydration reactions involving two neighboring carboxylic acids groups, two phenol groups, or a carboxylic acid and a phenol group [105,106,109,110]. In turn, the release of H_2 above around 650 °C is due to the occurrence of reactions of aromatization and condensation of aromatic rings [105,109–111]. Finally, the slight release of CH_4 that takes place in the range of ~550-900 °C is due to the presence of some aliphatic carbons.

Concerning the TPD of the sample that underwent complementary carbonization (WVC), one could foresee that it would not give rise to any emission below 800 °C because the material has already been heated up to this temperature. However, although in low intensity, WVC presented some CO_2 and CO emission below 800 °C (Figure 9). The explanation for this behavior is that carbon atoms with incomplete valencies and unpaired electrons are left behind after carbonization, and these atoms are able to react with atmospheric oxygen and water vapor to generate acidic oxygenated groups [112,113]. As would be expected, CO emissions were intensified above 800 °C due to the decomposition of carbonyl-containing groups.

In accordance with the above-described reactions that take place during complementary carbonization, WVC presented, in comparison to WV, lower H/C atomic ratio and O content, which decreased from 0.41 to 0.16 (Table 2) and from 13.6 to 8.4 wt% (Figure S2b; Table 3), respectively. In addition, both the acidic and basic contents decreased: from 1.11 to 0.19 mmol g^{-1} and from 0.45 to 0.32 mmol g^{-1}, respectively (Table 2). Finally, PZC increased from 4.7 to 6.2 (Table 2).

 doi:10.20944/preprints202501.0451.v1

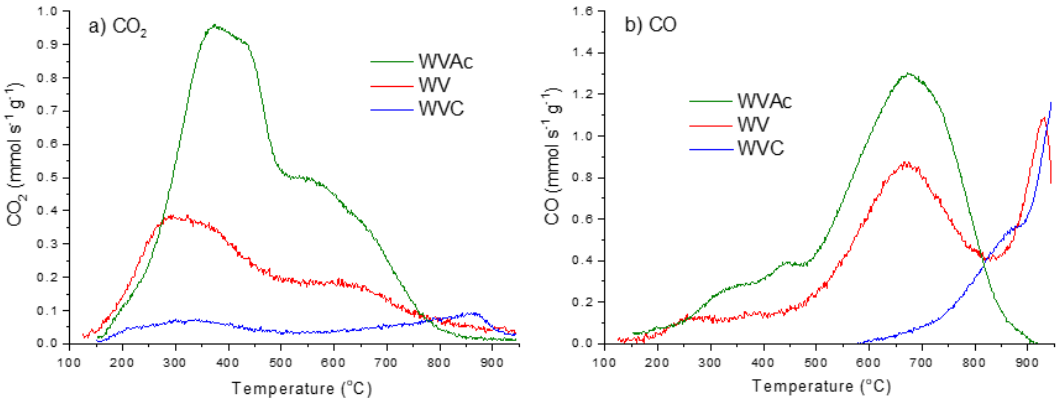

Figure 9. (a) CO_2 and (b) CO-TPD profiles of WV and the samples obtained from its complementary carbonization and nitrification.

Carboxylic acids and phenols are the main groups decomposed during complementary carbonization. The former has one OI and one OII type oxygen, while the latter has only one OII type oxygen. Therefore, the decomposition of phenolic groups explains why, in comparison to WV, WVC presented a lower relative contribution of the OII-peak for the O 1*s* XPS envelope (the values were 52.1 and 57.1% for WVC and WV, respectively; Table 4).

Another important change observed during the complementary carbonization of WV was a reduction in porosity: V_{mic} and V_{mes} decreased from 0.50 and 0.42 $cm^3\ g^{-1}$ to 0.43 and 0.32 $cm^3\ g^{-1}$, respectively (Table 1). Consequently, SSA also decreased, from 1508 to 1298 $m^2\ g^{-1}$. These results can be attributed to the aromatization and condensation of aromatic rings that took place during complementary carbonization, which caused a shrinkage of the material particles and, consequently, a contraction of pore dimensions. Similar results were reported elsewhere for the complementary carbonization of carbons chemically activated with H_3PO_4 and $ZnCl_2$ [114,115].

3.3. Nitrification

The treatment of WV with HNO_3 promoted a pronounced increase of the acidic content, from 1.11 to 1.94 mmol g^{-1}, whereas the content of basic groups became zero (Table 2). Accordingly, PZC pronouncedly decreased, from 4.7 to 1.8.

Concerning the TPD profiles (Figure 9), the intensity of all CO_2 emissions pronouncedly increased after nitrification, evidencing the creation of additional carboxylic acids, anhydrides and lactones. In turn, CO emissions intensified up to ~830 °C, which can be attributed to the creation of additional anhydride and phenol groups. However, the increase of CO emissions in the range of nearly 500-850 °C was less intense than the increase of CO_2 emissions, which evidences that nitrification led primarily to the formation of carboxylic groups. Indeed, Figueiredo et al. [22] have already reported that the treatment of an AC with HNO_3 decreased the ratio between the intensity of the CO and CO_2 TPD peaks.

Another interesting aspect to be noted is that CO emissions at higher temperatures (above ~830 °C) vanished after nitrification, which is in accordance with the null content of basic groups measured by titration for WVAc (Table 2). The consumption of the carbonyl groups can be attributed to the oxidative attack of HNO_3, which is a well know reaction [116].

HNO_3 treatment increased the O content (determined by XPS) from 13.6 to 17.0 wt% (Figure S2c; Table 3). In accordance with carbonyls oxidation and phenol formation, there was an increase in the relative contribution of the OII peak for the O 1*s* XPS envelope (the values were 63.0 and 57.1 wt% for WVAc and WV, respectively; Table 4). Furthermore, there was an increase in the N content, from 0.2/0.3 to 2.7/1.7 wt% [EA (Table 2)/XPS (Table 3)]. The HR N 1*s* core level spectrum (Figure 10) reveals

 doi:10.20944/preprints202501.0451.v1

that N was inserted as nitro groups (—NO_2), leading to a peak centered at 406 eV [35,71,79,94]. Finally, the Na present in the pristine AC WC was leached by the employed HNO_3 solution (Table 3).

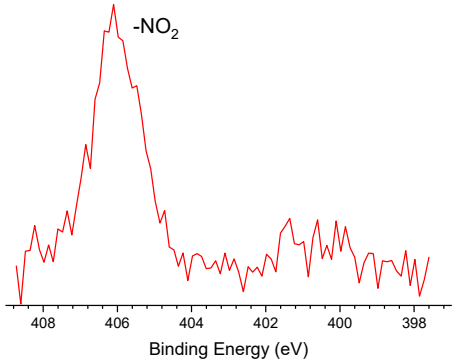

Figure 10. HR N 1*s* core level spectrum for the AC modified by nitrification.

Figure 4 and Table 1 portray that nitrification somewhat reduced the available porosity and SSA. This is a typical behavior that is commonly attributed to two factors: (i) the formation of acidic oxygenated groups that can block the entrance of some narrow pores; (ii) the collapse of some pore walls by oxidation [110,117,118]. In the present case, since nitrification was conducted under mild conditions (dilute HNO_3), we believe that the first reason was preponderant.

3.4. Ammonization

The results of EA (Table 2) and XPS (Figure S3; Table 3) show that ammonization up to both temperatures of 400 and 800 °C promoted the desired nitrogen incorporation. It is notable that there is a relatively good agreement between the N content determined through the different analytical methods. Considering that, as already mentioned in Subsection 3.1, XPS is a surface technique while EA is a bulk technique, these results can be taken as evidence that NH_3 diffused well throughout the carbon particles.

3.4.1. Ammonization up to 400 °C

Among the materials prepared by ammonized up to 400 °C, WVAcN400 presented the highest N content, 6.8/7.8 wt% [EA (Table 2)/XPS (Table 3)]. This material was produced from WVAc, the sample that had been pre-treated with HNO_3 and therefore had the highest content of oxygenated acidic groups among the materials submitted to ammonization. These findings suggest that N incorporation is favored by the presence of oxygenated acidic groups on the surface of the starting material. Indeed, Stohr et al. [119] proposed that, under heating, NH_3 reacts with carboxylic acid and phenol/ether groups to render amides and amines, respectively, as represented in Equations 1-3 of Figure 11. Furthermore, Ortega et al. [87] proposed that other carboxylic groups such as anhydrides and lactones also react with NH_3, as illustrated by Equations 4 and 5.

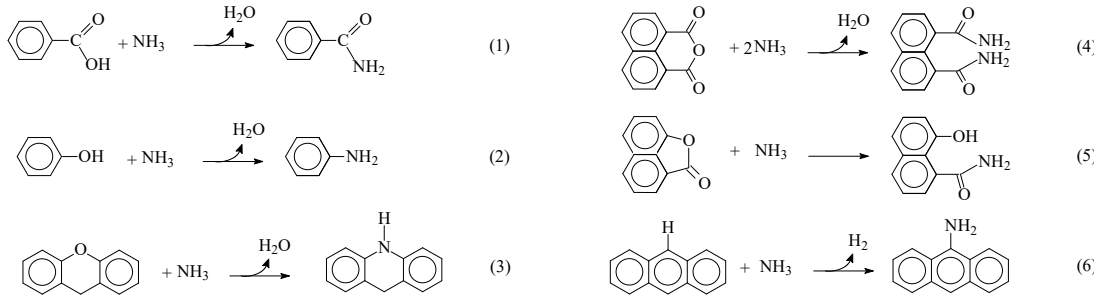

 doi:10.20944/preprints202501.0451.v1

Figure 11. Examples of hypothetical reactions of ACs with NH_3.

At this point, it is worth noting that WVCN400 presented a considerable N content, 2.8/3.1 wt% [EA (Table 2)/XPS (Table 3)], despite the low presence of oxygenated acidic groups in the starting material (WVC). This result evidences that there must exist another pathway for N incorporation that does not depend on the presence of oxygenated acidic groups. We speculate that the temperature of 400 °C is high enough to promote the insertion of $-NH_2$ groups (aminic nitrogen) directly onto the edge carbon atoms, as illustrated by Equation 6 in Figure 11. Then, the amides and amines formed as illustrated in Figure 11 would undergo a series of subsequent cyclization reactions, as shown in Equations 7-11 in Figure 12, some of which have already been suggested by other authors [87,90].

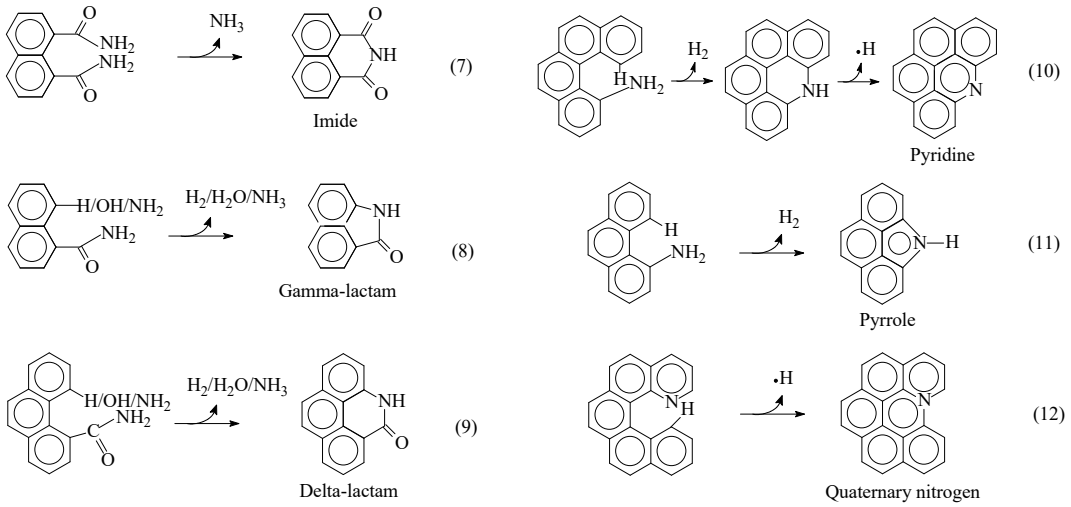

Figure 12. Examples of hypothetical cyclization reactions taking place during ammonization of ACs.

Some additional reactions have been described. For example, Arrigo et al. [25], Ortega et al. [87] and Arrigo et al. [88] proposed the decarbonilation of delta-lactams into pyrrole (Equations 13 in Figure 13). Furthermore, Arrigo et al. [25] proposed that the iminol tautomeric form of amide could lose H_2O to form pyridine (Equations 14 in Figure 13). Both reactions are plausible, but we do not have how to prove their occurrence.

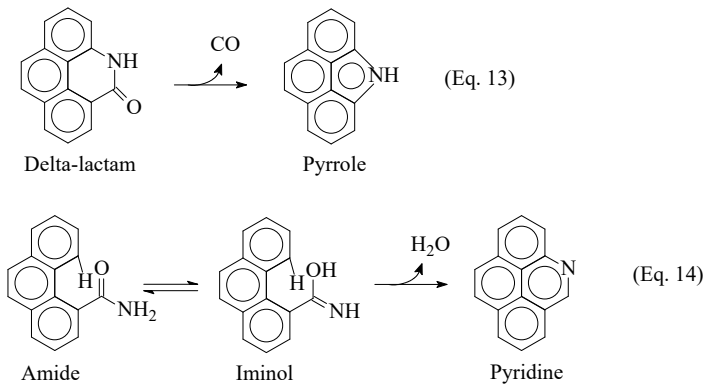

Figure 13. Additional hypothetical reactions that would take place during ammonization of ACs.

Figures 14a, 14c and 14e show the HR N 1*s* core level spectra of the samples ammonized up to 400 °C, which present an envelope between around 397 and 402 eV. In accordance with the literature and the above-proposed reactions, this envelope was deconvoluted into four contributions centered

 doi:10.20944/preprints202501.0451.v1

at around 398.5, 399.5, 400.3 and 401.5 eV. They were assigned, respectively, mainly to: pyridinic N (N-6 peak); aliphatic N (N-X peak) in amines, imides and lactams; pyrrolic N (N-5 peak); quaternary nitrogen (N-Q peak) [28,32,35,52,58,63,64,71,73,75,86,89]. Furthermore, some authors [21,59,86] have considered that the peak at around 400.3 eV (that is to say, N-5, according to the employed nomenclature) can also have contribution from pyridine-like structures, which are formed as tautomeric forms of delta-lactams (Figure 15). The presence of some N-Q could be explained by the occurrence of reactions such as that displayed by Equation 12 in Figure 12.

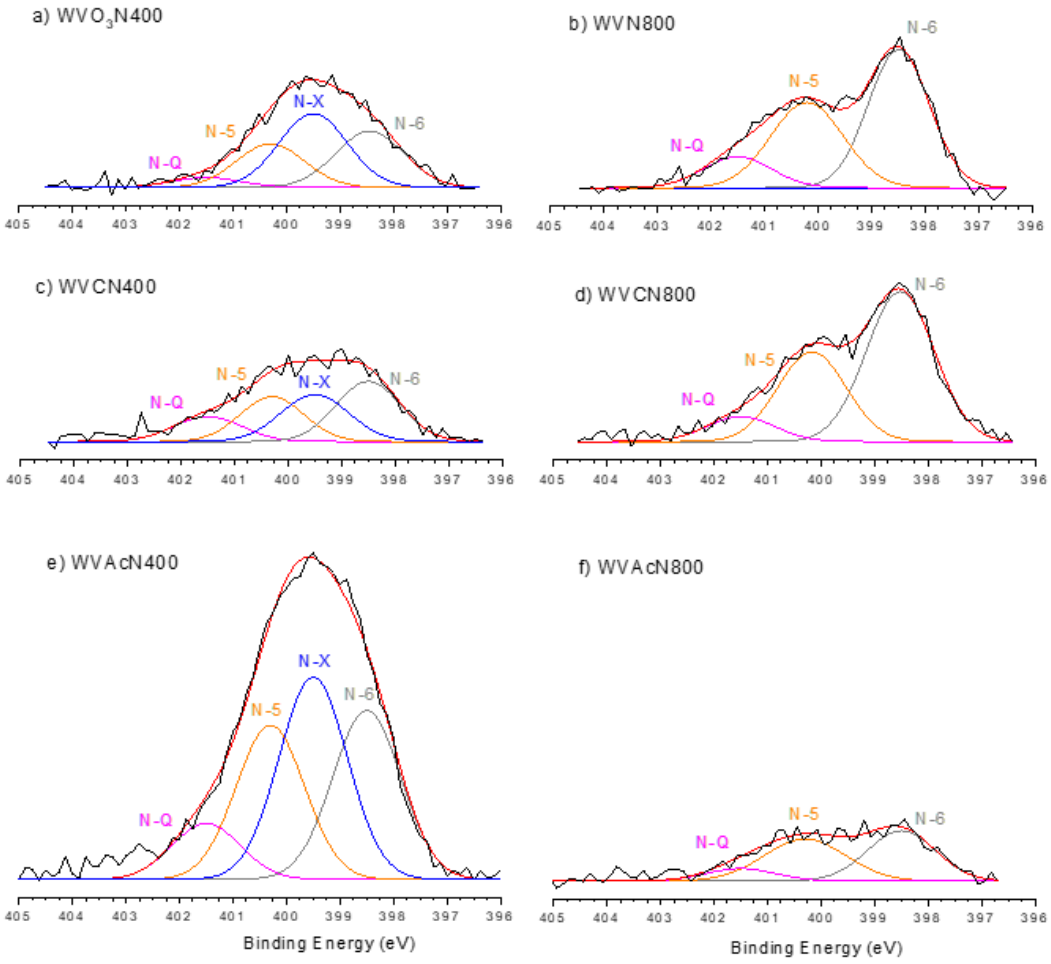

Figure 14. HR N 1*s* core level spectra for the ammonized ACs.

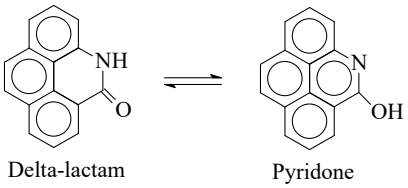

Figure 15. Tautomeric equilibrium between delta-lactam and pyridone-like structures.

It is worth to point out that the –NO_2 groups previously introduced by the nitrification treatment were completely removed during ammonization, as revealed by the absence of a peak between 404 and 408 eV in the HR N1*s* core level spectrum of WVAcN400.

Mass losses of 4.2 and 1.8 wt% took place during the ammonization procedures leading to WVN400 and WVAcN400, respectively, while a mass gain of 3.2 occurred during the ammonization

 doi:10.20944/preprints202501.0451.v1

that produced WVCN400 (Table 2). These results are in accordance with the idea that, for materials with a relatively high content of oxygenated acidic groups, N incorporation takes place primarily through the reactions described by Equations 1-5 in Figure 11, followed by reactions like those in Equations 7-9 in Figure 12 and Equations 13 and 14 in Figure 13. In general terms, these reactions release small molecules such as NH_3, CO, and H_2O, which would explain the slight weight losses observed during the ammonization of WV and WVAc up to 400 °C. On the other hand, in the case of samples with low content of oxygenated acidic groups, the initial incorporation of N would take place mainly through reactions like that presented by Equation 6 in Figure 11, followed by reactions like those illustrated by Equations 10-12 in Figure 12. The combination of these reactions would explain the small mass gain verified during the ammonization of WVC up to 400 °C.

In accordance with the proposed reactions, N incorporation during ammonization up to 400 °C was followed by reductions in O content: from 13.6 (WV) to 10.7 wt% (WVN400); from 8.4 (WVC) to 8.1 wt% (WVCN400); from 17.0 (WVAc) to 9.5 wt% (WVAc400) (Table 3). In the case of WVC, the reduction was slight because, as discussed above, the main route for N incorporation did not involve the consumption of oxygenated groups. In turn, since WVAc presented, among the samples submitted to ammonization, the higher content of oxygenated groups, it underwent the largest reduction in O content.

As expected, the ammonization of the materials having relatively high content of oxygenated acidic groups up to 400 °C increased PZC: from 4.7 (WV) to 6.8 (WVN400) and from 1.8 (WVAc) to 3.4 (WVAcN400) (Table 2). On the other hand, in the case of the material that did not display elevated content of oxygenated acidic groups, WVC, its PZC near the neutrality (6.2) was not significantly altered (the PZC measured for WVC400 was 6.1).

Figure 16 shows the CO_2- and CO-TPD profiles of the samples ammonized up to 400 °C. It is notable that the CO profiles were very similar to those of the corresponding materials before ammonization (Figure 9). In this sense, the presence of an intense peak in the ~500-850 °C region for the samples WVN400 and WVAcN400 can be taken as evidence that the conversion of phenol/ether groups into amines according to Equations 2 and 3 in Figure 11 was not prominent during ammonization up to 400 °C. In this sense, it is valid to highlight that the remnant of phenolic groups would be able to explain the considerable acidic content verified for the referred samples (0.50 and 1.06 mmol g^{-1}, respectively).

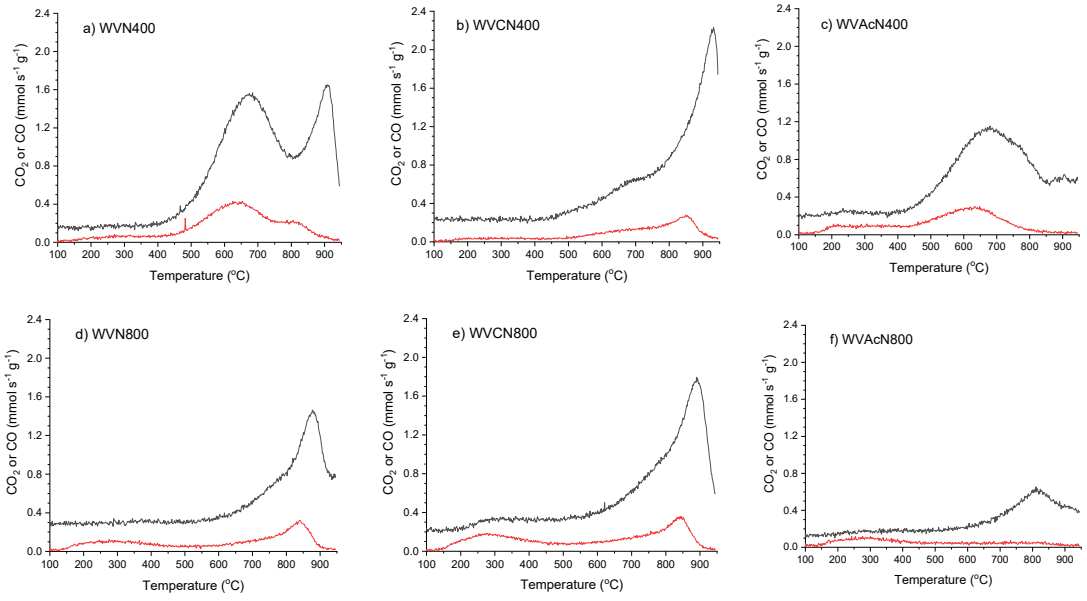

Figure 16. CO_2 (red lines) and CO-TPD (black lines) profiles of ammonized samples (the scale was kept the same in order to facilitate comparisons).

 doi:10.20944/preprints202501.0451.v1

In turn, the CO_2-TPD profile was completely modified by ammonization up to 400 °C. Below ~450 °C, CO_2 emissions practically disappeared because, as discussed above, carboxylic acids reacted with NH_3 or even decomposed. On the other hand, CO_2 release was intensified in the range of ~500-900 °C, which is somewhat surprising because, as already discussed in Subsection 3.1, CO_2, as a rule, is released only by the decomposition of carboxylic groups in the low to medium temperature range. An interesting aspect to be noted is that the CO_2-TPD profile of the samples ammonized up to 400 °C seems to correlate with the corresponding CO profile in the medium-to-high temperature range. For example, samples WVN400 and WVAcN400 present a large CO_2 emission between around 450 and 800 °C, which resembles the CO emission in this temperature range. Concerning higher temperatures, it is notable that the samples that released CO above ~800 °C (WVN400 and WVCN400) also released some CO_2 in the ~800-900 °C range, whereas the sample that did not emit CO above ~800 °C (WVAcN400) also did not emit any CO_2. These results strongly suggest that at least most of the CO_2 detected during TPD analyses of ammonized samples would actually be the result of a partial conversion of the released CO to CO_2 within the sample holder (the so-called inverse Boudouard reaction [107]).

At this point, it is worth mentioning that the lactone decomposes in the range of ~500-900 °C (Figure 8). However, it is assumed that the lactones reacted with NH_3 during ammonization and the intensity; furthermore, the CO_2 emissions in the range of ~500-900 °C were even more intense for the materials ammonized up to 400 °C than for the corresponding materials before ammonization (compare the CO_2-TPD profiles of samples WVN400 and WVAc400 in Figures 16 a and 16c with those of samples WVN and WVAc in Figure 9a).

Marchon et al. [119] proposed that the conversion of CO to CO_2 involves the reaction of a carbonyl group with CO to give a lactone, which would decompose in the sequence to release CO_2. A possible mechanism to explain this reaction is proposed in Figure 17. Since the conversion of CO into CO_2 was significantly observed only for ammonized samples, it is possible to infer that the referred conversion is favored by the presence of N-containing groups. This hypothesis is in accordance with the proposed mechanism since, as portrayed in Figure 2, N-containing groups increase the density of π electrons on the carbon basal planes, which would increase the contribution of the resonant structure (II) of Figure 17 to the overall hybrid structure and therefore favor the nucleophilic attach of carbonylic oxygen to a CO molecule.

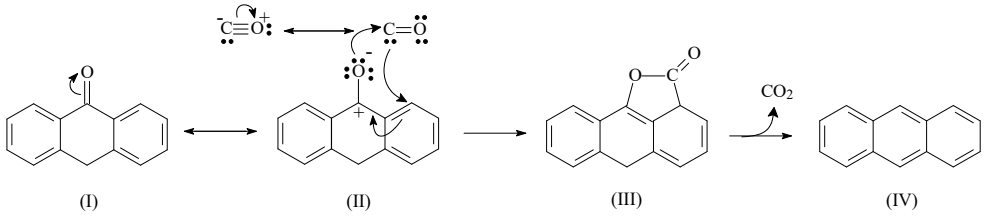

Figure 17. Possible mechanism to explain the CO conversion into CO_2.

An additional point that is worth addressing here is that the relative intensity between CO_2 emission and the corresponding CO emission became lower the higher the temperature. Thus, for example, while CO emissions for WVN400 had two well defined intense maxima around 675 and 910 °C, the corresponding CO_2 emissions presented a maximum at 640 °C with a kind of elbow at ~810 °C (Figure 16a). This behavior can be understood in light of the mechanism proposed above for the conversion of CO into CO_2: firstly, because the nitrogenated groups, which favors the conversion, gradually decompose as the temperature increases, which would contribute to decrease the rate of CO conversion; secondly, because the carbonyl groups that promotes the conversion start to decompose above ~800 °C (remember that the CO to be converted at higher temperatures is formed precisely by the decomposition of carbonyls).

 doi:10.20944/preprints202501.0451.v1

Figure 18 and the data in Table 1 show that the ammonization of WV and WVAc up to 400 °C reduced the porosity of the materials, while the porosity changed little in the case of the ammonization of the sample that had previously been submitted to complementary carbonization (WVC). This behavior shows that N-containing groups inserted during ammonization reduce the available porosity in the materials that are still in an incipient carbonization degree (that is to say, that were not heated at relatively high temperatures such as 800 °C).

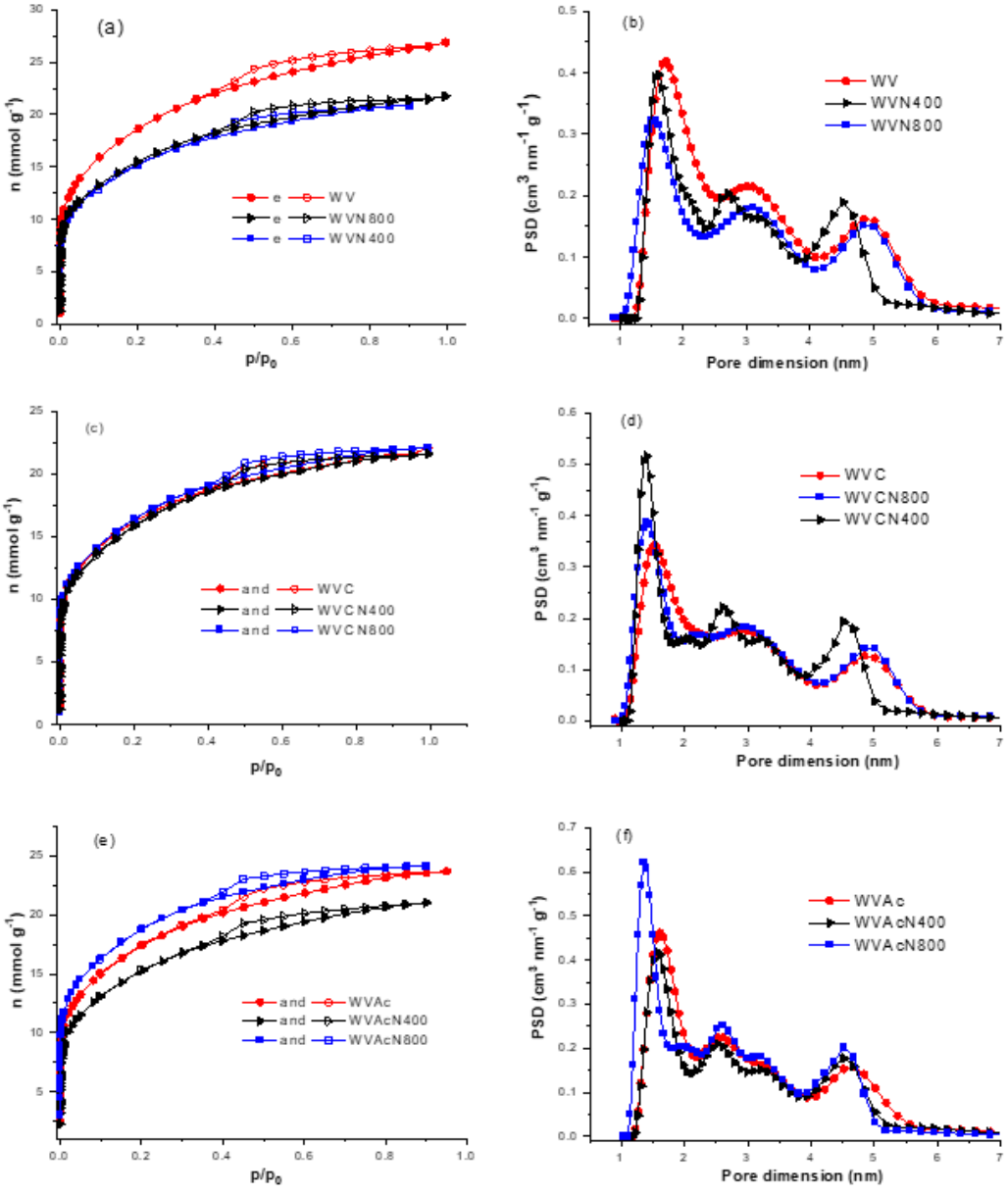

Figure 18. (a) N_2 adsorption-desorption isotherms of the ammonized samples and (b) the corresponding PSD curves (for the sake of comparison, the isotherms and PSD curves of the respective starting materials were included; closed and open symbols correspond to the adsorption and desorption branches, respectively).

3.4.2. Ammonization up to 800 °C

Increasing the maximum ammonization temperature from 400 to 800 °C caused different effects on N incorporation depending on the chemical composition of the starting material. For the unmodified AC (WV) and the sample that had previously been submitted to complementary

 doi:10.20944/preprints202501.0451.v1

carbonization (WVC), the N incorporation during ammonization up to 800 °C was higher than during ammonization up to 400 °C. The N contents were 5.5/5.1 and 3.5/3.9 wt% for WVN800 and WVCN800, respectively, whereas the values for their counterparts ammonized up to 400 °C were 3.9/3.1 and 2.8/31 [EA (Table 2)/XPS (Table 3)]. Additional incorporation of nitrogen above 400 °C is assumed to occur due to the reaction of NH_3 (or derived species such as $\cdot NH_2$ radicals) with the edge carbons in a manner similar to that illustrated by Equation 6 in Figure 11.

On the other hand, for the sample that had been previously treated with HNO_3 (WVAc), the effect of increasing the ammonization temperature was contrary, so that WVAcN800 presented a much lower N content than WVAcN400 [the values were 1.6/1.9 and 7.8/6.8 wt%, respectively; EA (Table 2)/XPS (Table 3)]. These results can be related to the intense weight loss verified during the ammonization of WVAc up to 800 °C, 32.4% (Table 2), and shows that, if on the one hand the presence of oxygenated acidic groups favors N incorporation at low-to-medium temperatures, on the other hand the resulting structure is highly susceptible to decomposition at higher temperatures, leading therefore to the release of most of the N incorporated at lower temperatures. For the sake of comparison, the respective weight losses during the ammonization of WV and WVC were only 10.8 and 1.5%, respectively.

The HR N1*s* core level spectra of the samples ammonized up to 800 °C presented different profiles than those verified for their counterparts ammonized up to 400 °C (compare Figures 14b with 14a, 14d with 13c, and 14f with 14e). The N-X peak due to aliphatic nitrogen, which was prominent for the samples ammonized up to 400 °C, was not present in the spectra of the samples ammonized up to 800 °C. For the latter, only aromatic nitrogens, mainly pyrrolic (N-5) and pyridinic (N-6), are present. At this point it is worth highlighting that a similar trend can be observed in the N 1*s* core level spectra of the materials prepared through ammonization up to different temperatures by other authors [25,52,76,88]. In this sense, Arrigo et al. [25] reported N-X contents (called in their work N2 peak) of 5.0, 6.7 and 0.0 for materials obtained by ammonization up to 200, 400 and 600 °C, respectively, of a carbon nanofiber pre-treated with HNO_3 (concentrated, 120 °C, 2 h).

As expected, the TPDs of the samples ammonized up to 800 °C (Figure 16d-16f) presented low CO and CO_2 emission up to this temperature. Similar to the material submitted to complementary carbonization (Subsection 3.2), the minor emissions that took place bellow the maximum temperature reached during the material processing are attributed to functional groups formed by post-synthesis reaction with atmospheric O_2 and H_2O. In turn, the intense CO emission peak verified for WVN800 and WVCN800 at around 880-890 °C is assigned to the decomposition of carbonyl groups. In the case of WVAcN800, this emission is not observed because, as already discussed in Subsection 3.3, the carbonyl groups were consumed by the pre-treatment with HNO_3. It is noteworthy that, in the same way as verified for the samples ammonized up to 400 °C, the CO emissions from the samples ammonized up to 800 °C had a corresponding less intense evolution of CO_2, supposedly due to the conversion of CO into CO_2 (see pertinent discussion in Subsection 3.4.1).

The samples ammonized up to 800 °C presented a lower O content than the corresponding starting materials and counterparts ammonized up to 400 °C. The values were 13.6/10.7/7.2% for WV/WVN400/WVN800, 8.4/8.1/7.6% for WVC/WVCN400/WVCN800, and 17.0/9.5/8.2% for WVAc/WVAcN400/WVAcN800 (Table 2). In the case of the series WVC/WVCN400/WVCN800, the reduction was slight because WVC had already lost the labile oxygenated groups during the previous complementary carbonization. Furthermore, WVN800 and WVAcN800 had considerably higher aromaticity due to the thermal effects during ammonization. The H/C ratios were: 0.41/0.39/0.29 for WV/WVN400/WVN800; 0.48/0.50/0.19 for WVAc/WVAcN400/ WVAcN800. In the case of WVC, as it had already been treated at 800 °C during complementary carbonization, no additional gain of aromaticity was detected after ammonization. The determined H/C ratios were 0.16/0.15/0.19 for WVC/WVCN400/WVCN800.

As expected, the materials ammonized up to 800 °C presented a higher content of basic groups than acidic groups. The acidic/basic contents were 0.33/0.75, 0.07/0.86 and 0.32/0.68 mmol g^{-1} for

 doi:10.20944/preprints202501.0451.v1

WVN800, WVCN800 and WVAcN800, respectively. Even though, the corresponding measured PZC values were always near neutrality: 6.2, 6.3 and 6.9.

Concerning the textural properties, it is first necessary to stress that, for materials that have not been previously processed at high temperatures (the cases of WV and WVAc), it would be expected that the increase of the maximum ammonization temperature from 400 to 800 °C would have provoked a porosity shrinkage due to thermal effects, in a similar way as verified when WV was submitted to complementary carbonization (Subsection 3.2). However, this behavior was not observed in the present study (Figure 18; Table 1). Instead, in the case of sample WWN800, the porosity was much similar to that of its counterpart ammonized up to 400 °C (WWN400). In turn, the porosity of WWAcN800 was much higher than that of its counterpart sample ammonized up to 400 °C (WWAcN400). These findings evidence that another effect balanced or even surpassed the trend of porosity shrinkage due to thermal issues. This effect is supposed to be the above-mentioned degradation, in the medium-to-high temperature range, of labile aliphatic N-containing functionalities formed at lower temperatures. As reported at the end of the previous Subsection, these functionalities would reduce the available porosity of the sample ammonized up to 400 °C, so that their removal would work as a kind of "material gasification" that increases the available porosity.

As expected, none of the above reported effects were relevant in the case of WVC ammonization. Firstly, because this material had already been previously processed at high temperature during the complementary carbonization, so that the thermal effect of porosity shrinkage had already taken place (see Subsection 3.2). Secondly because, since WVC had a low content of oxygenated acidic groups, the formation of labile aliphatic N-containing functionalities was not significant during its ammonization (see pertinent discussions in Subsection 3.4.1). Therefore, the sample WVCN800 had a very similar porosity to its counterpart ammonized up to 400 °C (WWCN400).

3.4.3. Final Considerations About Ammonization

Although there are scarce works in the literature concerning the ammonization of carbon-based materials at (or up to) different temperatures, the results of the existing works are in consonance with those presented here. These works can be divided into two groups. The first group corresponds to those works whose authors carried out the direct ammonization of carbon materials, that is to say, without performing an oxidative pre-treatment [37,39,52]. For these authors, the content of N incorporated at higher temperatures was higher, in a similar manner as verified for the ammonization of WV and WVC in the present work. For example: Pevida et al. [37] reported N contents (EA) of 3.3 and 6.3 wt% for the materials obtained through ammonization at 400 and 800 °C (2 h), respectively, of a commercial H_3PO4 activated carbon; Yang et al. [52] reported N contents (XPS) of 1.03 and 2.80 wt% for the materials obtained through ammonization up to 350 and 850 °C (2 h), respectively, of a commercial AC. In the other group are the works whose authors carried out a pre-treatment of the carbon material with HNO_3 before ammonization [25,76,87,88]. For these authors, the content of N incorporated at higher temperatures was lower, in a similar manner as verified for the ammonization of WVAc in the present work. For example: Zhang et al. [76] reported N contents (EA) of 4.0 and 2.1 wt% for the materials obtained through ammonization at 400 and 800 °C (2 h), respectively, of the materials obtained through chemical activation of a petroleum coke with KOH followed by pre-treatment with a HNO_3 solution (20 wt%, 3 h, 60 °C); Kundu et al. [88] reported N contents (XPS) of 3.5 and 1.1 wt% for the materials obtained through ammonization at 400 and 800 °C (2 h), respectively, of materials obtained through pre-treatment of commercial carbon nanotubes with HNO_3 vapor (48 h, 200 °C).

It is should also be mentioned that some authors have inadvertently carried out an oxidative pre-treatment with HNO_3 prior to ammonization [25,50,76,87,88], based on the premise that this pre-treatment improve N incorporation. However, the results reported in the present work show that the effects of pretreatment of a carbon-based material on N-incorporation depend on the ammonization temperature and the surface chemical composition of the starting material. Therefore, the pertinence of carrying out a nitrification pre-treatment should be evaluated on a case-by-case basis.

 doi:10.20944/preprints202501.0451.v1

 doi:10.20944/preprints202501.0451.v1

4. Conclusions

The present work provides valuable insights on the preparation of N-doped ACs through ammonization. The results showed that, during ammonization up to low temperatures (around 400 ºC), nitrogen is incorporated in the form of aliphatic (supposedly amines, imides and lactams), pyridinic and pyrrolic groups, with a minor contribution of quaternary nitrogen. The presence of oxygenated acidic groups (mainly carboxylic acids, anhydrides and lactones) on the surface of the starting material favors N insertion by means of the formation of amides that, in the sequence, undergo cyclization reactions to give rise mainly to imides and lactams. Therefore, the highest N content on the AC surface (around 8 wt%, as determined by XPS) was verified for the sample obtained from ammonization up to 400 ºC of the material that had been pre-treated with a HNO_3 solution (because this pre-treatment greatly increased the content of the referred oxygenated acidic groups).

Although the presence of oxygenated acidic groups favors N incorporation, it is not an indispensable requisite, because NH_3 can alternatively react directly with edge carbon atoms, presumably to give rise to amine groups that can react in the sequence to form mainly pyridine and pyrrole-like structures. Therefore, even the sample that had been submitted to a previous complementary carbonization up to 800 ºC, which presented a quite low content of oxygenated acidic groups, incorporated considerable content of N during ammonization up to 400 ºC (around 3 wt%, as determined by XPS).

By increasing the maximum ammonization temperature to 800 ºC, two effects were observed: (i) on the one hand, the incorporation of N was favored; (ii) on the other hand, reaching high temperatures provoked the decomposition of aliphatic groups, which caused the release of part of the N that had been incorporated at lower temperatures. The overall result was that the N present in the materials obtained by ammonization up to 800 ºC was found only in the form of aromatic N, mainly pyridinic and pyrrolic ones, with a minor contribution of quaternary N. Furthermore, if the starting material had a high content of oxygenated acidic groups, the N content of the material obtained after ammonization up to 800 ºC was lower than that verified for its counterpart material ammonized up to 400 ºC, because most of the N was incorporated in the form of aliphatic groups that decomposed at higher temperatures. In turn, if the starting material had a low-to-medium content of oxygenated acidic groups, the N content verified for the materials prepared by ammonization up to 800 ºC was superior to that verified for their counterpart samples ammonized up to 400 ºC, because a larger amount of N was incorporated in the form of stable aromatic rings.

Supplementary Materials: The following supporting information can be downloaded at the website of this paper posted on Preprints.org

Author Contributions: Conceptualization and methodology, M.J.P. and E.R.-C.; funding acquisition, M.J.P., E.R.-C. and A.M.A.S.; supervision, M.J.P; Resources, J.J.L.L., G.A.V.M. and D.C.S.D.A.; Formal analysis, M.J.P., G.A.V.M., J.J.L.L., S.D.C.O., R.C.D., R.G.S, D.B.-P and E.R.-C.; Investigation, S.D.C.O., R.G.S., R.C.D. and D.B.-P; writing—original draft preparation, M.J.P.; Writing—review & editing, S.D.C.O., E.R.-C. and D.B.-P.

Funding: M.J.P., R.C.D. and A.M.A.S. thanks FINEP (Funder of Studies and Projects, Brazil; contractual instrument 01.23.0594.00) for the financial support to this research. D.B.-P and E.R.-C. thank to Spanish Ministry of Science and Innovation, project PID2021-126235OB-C32 funded by MCIN/ AEI/10.13039/501100011033/ and FEDER funds, and project TED2021-130756B-C31 funded by MCIN/AEI/10.13039/501100011033 and by "ERDF A way of making Europe" by the European Union Next Generation EU/PRTR. All authors thank CAPES (Brazilian Federal Agency for Support and Evaluation of Graduate Education, Brazil; Finance Code 001) for the financial support to this research.

Conflicts of Interest: The authors declare no conflicts of interest.

 doi:10.20944/preprints202501.0451.v1

References

1. Thommes, M.; Kaneko, K.; Neimark, A.V.; Olivier, J.P.; Rodriguez-Reinoso, F.; Rouquerol, J.; Sing, K.S.W. Physisorption of gases, with special reference to the evaluation of surface area and pore size distribution (IUPAC Technical Report). *Pure Appl. Chem.* **2015**, *87*, 1051–1069.
2. Zieliński, B.; Miądlicki, P.; Przepiórski, J. Development of activated carbon for removal of pesticides from water: case study. *Sci. Rep.* **2022**, *12*, 20869.
3. Kumar, N.; Pandey, A.; Rosy; Sharma, Y.C.A. Review on sustainable mesoporous activated carbon as adsorbent for efficient removal of hazardous dyes from industrial wastewater. *J. Water Process Eng.* **2023**, *54*, 104054.
4. Enterría, M.; Figueiredo, J.L. Nanostructured mesoporous carbons: tuning texture and surface chemistry. *Carbon* **2016**, *108*, 79–102.
5. Novaes, H.R.; Prauchner, M.J.; Ginoris, Y.P. Cylindrospermopsin adsorption onto activated carbons synthesized from coconut shell: effect of surface chemical composition on removal efficiency. *Adsorpt. Sci. Technol.* **2024**, *42*.
6. Ferrero, G.A.; Fuertes, A.B.; Sevilla, M.; Titirici, M.-M. Efficient metal-free n-doped mesoporous carbon catalysts for ORR by a template-free approach. *Carbon* **2016**, *106*, 179–187.
7. *Activated Carbon: Progress and Applications*; Verma, C., Quraishi, M.A., Eds.; The Royal Society of Chemistry, 2023.
8. Marsh, H.; Rodríguez-Reinoso, F. *Activated Carbon*; Elsevier, 2006.
9. Zhao, C.; Ge, L.; Mai, L.; Li, X.; Chen, S.; Li, Q.; Li, S.; Yao, L.; Wang, Y.; Xu, C. Review on coal-based activated carbon: preparation, modification, application, regeneration, and perspectives. *Energy & Fuels* **2023**, *37*, 11622–11642.
10. Reza, M.S.; Yun, C.S.; Afroze, S.; Radenahmad, N.; Bakar, M.S.A.; Saidur, R.; Taweekun, J.; Azad, A.K. Preparation of activated carbon from biomass and its' applications in water and gas purification, a review. *Arab J. Basic Appl. Sci.* **2020**, *27*, 208–238.
11. Kasera, N.; Kolar, P.; Hall, S.G. Nitrogen-doped biochars as adsorbents for mitigation of heavy metals and organics from water: a review. *Biochar* **2022**, *4*, 17.
12. Snezhkova, E.; Redl, H.; Grillari, J.; Osuchowski, M. Activated carbon for sepsis prevention and intervention: a modern way of utilizing old therapies. *C* **2023**, *9*, 72.
13. Miriyala, N.; Ouyang, D.; Perrie, Y.; Lowry, D.; Kirby, D. J. Activated carbon as a carrier for amorphous drug delivery: effect of drug characteristics and carrier wettability. *Eur. J. Pharm. Biopharm.* **2017**, *115*, 197–205.
14. Choi, J.-S.; Lim, S.-H.; Lingamdinne, L.P.; Park, S.-Y.; Koduru, J.R.; Yang, J.-K.; Chang, Y.-Y. Development of ultra-high surface area polyaniline-based activated carbon for the removal of volatile organic compounds from industrial effluents. *Environ. Pollut.* **2023**, *337*, 122594.
15. Tolkou, A.K.; Maroulas, K.N.; Theologis, D.; Katsoyiannis, I.A.; Kyzas, G.Z. Comparison of modified peels: natural peels or peels-based activated carbons for the removal of several pollutants found in wastewaters. *C* **2024**, *10*, 22.
16. Al-Hajri, W.; De Luna, Y.; Bensalah, N. Review on recent applications of nitrogen-doped carbon materials in CO_2 capture and energy conversion and storage. *Energy Technol.* **2022**, *10*, 2200498.
17. Chaudhary, R.; Maji, S.; Shrestha, R.G.; Shrestha, R.L.; Shrestha, T.; Ariga, K.; Shrestha, L.K. Jackfruit seed-derived nanoporous carbons as the electrode material for supercapacitors. *C* **2020**, *6*, 73.
18. Kumar Mishra, R.; Singh, B.; Acharya, B. A Comprehensive review on activated carbon from pyrolysis of lignocellulosic biomass: an application for energy and the environment. *Carbon Resour. Convers.* **2024**, *7*, 100228.
19. Yang, J.; Fu, L.; Wu, F.; Chen, X.; Wu, C.; Wang, Q. Recent developments in activated carbon catalysts based on pore size regulation in the application of catalytic ozonation. *Catalysts* **2022**, *12*, 1085.
20. Iwanow, M.; Gärtner, T.; Sieber, V.; König, B. Activated carbon as catalyst support: precursors, preparation, modification and characterization. *Beilstein J. Org. Chem.* **2020**, *16*, 1188–1202.
21. Figueiredo, J.L.; Pereira, M.F.R. The role of surface chemistry in catalysis with carbons. *catal. Today* **2010**, *150*, 2–7.

 doi:10.20944/preprints202501.0451.v1

22. Figueiredo, J.L.; Pereira, M.F.R.; Freitas, M.M.A.; Orfao, J.J.M. Modification of the surface chemistry of activated carbons. **1999**, *37*, 1379–1389
23. Rocha, R.P.; Pereira, M.F.R.; Figueiredo, J.L. Characterisation of the surface chemistry of carbon materials by temperature-programmed desorption: an assessment. *Catal. Today* **2023**, *418*, 114136.
24. Rocha, R.; Soares, O.; Figueiredo, J.; Pereira, M. Tuning CNT Properties for metal-free environmental catalytic applications. *C* **2016**, *2*, 17.
25. Arrigo, R.; Hävecker, M.; Wrabetz, S.; Blume, R.; Lerch, M.; McGregor, J.; Parrott, E.P.J.; Zeitler, J.A.; Gladden, L.F.; Knop-Gericke, A.; Schlögl, R.; Su, D.S. Tuning the acid/base properties of nanocarbons by functionalization via amination. *J. Am. Chem. Soc.* **2010**, *132*, 9616–9630.
26. Pietrzak, R. XPS study and physico-chemical properties of nitrogen-enriched microporous activated carbon from high volatile bituminous coal. *Fuel* **2009**, *88*, 1871–1877.
27. Shafeeyan, M.S.; Daud, W.M.A.W.; Houshmand, A.; Shamiri, A. A review on surface modification of activated carbon for carbon dioxide adsorption. *J. Anal. Appl. Pyrolysis* **2010**, *89*, 143–151.
28. Rehman, A.; Park, S.-J. Comparative study of activation methods to design nitrogen-doped ultra-microporous carbons as efficient contenders for CO_2 capture. *Chem. Eng. J.* **2018**, *352*, 539–548.
29. Wang, J.; Senkovska, I.; Oschatz, M.; Lohe, M.R.; Borchardt, L.; Heerwig, A.; Liu, Q.; Kaskel, S. Highly porous nitrogen-doped polyimine-based carbons with adjustable microstructures for CO_2 capture. *J. Mater. Chem. A* **2013**, *1*, 10951–10961.
30. Staciwa, P.; Sibera, D.; Pełech, I.; Narkiewicz, U.; Moszyński, D. CO_2 adsorption studies on spherical carbon derived from resorcinol-formaldehyde resin and sugars. *J. Environ. Chem. Eng.* **2024**, *12*, 111735.
31. Li, Y.; Zhang, G.; Wu, C.; Liu, J.; Li, G.; Wang, Y.; Zhao, Y. Novel nitrogen-enriched activated carbon with tunable microporosity from agricultural and plastic waste for CO_2 adsorption. *J. Environ. Chem. Eng.* **2023**, *11*, 111257.
32. Lee, M.-S.; Park, M.; Kim, H.Y.; Park, S.-J. Effects of microporosity and surface chemistry on separation performances of N-containing pitch-based activated carbons for CO_2/N_2 binary mixture. *Sci. Rep.* **2016**, *6*, 23224.
33. Bai, J.; Huang, J.; Yu, Q.; Demir, M.; Kilic, M.; Altay, B.N.; Hu, X.; Wang, L. N-doped porous carbon derived from macadamia nut shell for CO_2 adsorption. *Fuel Process. Technol.* **2023**, *249*, 107854.
34. Spessato, L.; Duarte, V.A.; Fonseca, J.M.; Arroyo, P.A.; Almeida, V.C. Nitrogen-doped activated carbons with high performances for CO_2 adsorption. *J. CO_2 Util.* **2022**, *61*, 102013.
35. Zhang, S.; Zhou, Q.; Jiang, X.; Yao, L.; Jiang, W.; Xie, R. Preparation and evaluation of nitrogen-tailored hierarchical meso-/micro-porous activated carbon for CO_2 adsorption. *Environ. Technol.* **2020**, *41*, 3544–3553.
36. Przepiórski, J.; Skrodzewicz, M.; Morawski, A.W. High temperature ammonia treatment of activated carbon for enhancement of CO_2 adsorption. *Appl. Surf. Sci.* **2004**, *225* (1–4), 235–242.
37. Pevida, C.; Plaza, M.G.; Arias, B.; Fermoso, J.; Rubiera, F.; Pis, J.J. Surface Modification of Activated Carbons for CO_2 capture. *Appl. Surf. Sci.* **2008**, *254*, 7165–7172.
38. Shafeeyan, M.S.; Daud, W.M.A.W.; Houshmand, A.; Arami-Niya, A. Ammonia modification of activated carbon to enhance carbon dioxide adsorption: effect of pre-oxidation. *Appl. Surf. Sci.* **2011**, *257*, 3936–3942.
39. Plaza, M.G.; Pevida, C.; Arias, B.; Fermoso, J.; Casal, M.D.; Martín, C.F.; Rubiera, F.; Pis, J.J. Development of low-cost biomass-based adsorbents for postcombustion CO2 capture. *Fuel* **2009**, *88*, 2442–2447.
40. Plaza, M.G.; Rubiera, F.; Pis, J.J.; Pevida, C. Ammoxidation of carbon materials for CO_2 capture. *Appl. Surf. Sci.* **2010**, *256*, 6843–6849.
41. Bezerra, D. P.; Silva, F. W. M. da; de Moura, P. A. S.; Sapag, K.; Vieira, R. S.; Rodriguez-Castellon, E.; de Azevedo, D. C. S. Adsorption of CO_2 on Amine-Grafted Activated Carbon. *Adsorpt. Sci. Technol.* **2014**, *32* (2–3), 141–151.
42. Li, T.; An, X.; Fu, D. Review on nitrogen-doped porous carbon materials for CO_2 adsorption and separation: recent advances and outlook. *Energy & Fuels* **2023**, *37*, 8160–8179.
43. Rashidi, N.A.; Yusup, S. An overview of activated carbons utilization for the post-combustion carbon dioxide capture. *J. CO_2 Util.* **2016**, *13*, 1–16.
44. Hu, W.; Huang, J.; Wang, J.; Xie, D.; Wang, Z.; Qiao, Y.; Xu, M. Benign-by-design N-doped activated carbon from wasted aqueous assisted hydrochar of leftover rice for efficient H_2S removal. *Fuel* **2024**, *358*, 130233.

 doi:10.20944/preprints202501.0451.v1

45. Bagreev, A.; Angel Menendez, J.; Dukhno, I.; Tarasenko, Y.; Bandosz, T.J. Bituminous coal-based activated carbons modified with nitrogen as adsorbents of hydrogen sulfide. *Carbon* **2004**, *42*, 469–476.
46. Chu, B.; Amano, Y.; Machida, M. Preparation of bean dreg derived N-doped activated carbon with high adsorption for Cr(VI). *Colloids Surfaces A Physicochem. Eng. Asp.* **2020**, *586*, 124262.
47. Yuan, X.; An, N.; Zhu, Z.; Sun, H.; Zheng, J.; Jia, M.; Lu, C.; Zhang, W.; Liu, N. Hierarchically porous nitrogen-doped carbon materials as efficient adsorbents for removal of heavy metal ions. *Process Saf. Environ. Prot.* **2018**, *119*, 320–329.
48. Guo, S.; Wang, Y.; Wei, X.; Gao, Y.; Xiao, B.; Yang, Y. Structural analysis and heavy metal adsorption of N-doped biochar from hydrothermal carbonization of *Camellia sinensis* Waste. *Environ. Sci. Pollut. Res.* **2020**, *27*, 18866–18874.
49. Bakry, A.M.; Awad, F.S.; Bobb, J.A.; El-Shall, M.S. Multifunctional binding sites on nitrogen-doped carboxylated porous carbon for highly efficient adsorption of Pb(II), Hg(II), and Cr(VI) ions. *ACS Omega* **2020**, *5*, 33090–33100.
50. Kasnejad, M. H.; Esfandiari, A.; Kaghazchi, T.; Asasian, N. Effect of pre-oxidation for introduction of nitrogen containing functional groups into the structure of activated carbons and its influence on Cu (II) adsorption. *J. Taiwan Inst. Chem. Eng.* **2012**, *43*, 736–740.
51. Smith, V.A.; Rivera, J.F.A.; Bello, R.; Rodríguez-Aguado, E.; Elshaer, M.R.; Wodzinski, R. L.; Bashkova, S. The role of surface chemistry and polyethylenimine grafting in the removal of Cr (VI) by activated carbons from cashew nut shells. *C* **2021**, *7*, 27.
52. Yang, G.; Chen, H.; Qin, H.; Feng, Y. Amination of activated carbon for enhancing phenol adsorption: effect of nitrogen-containing functional groups. *Appl. Surf. Sci.* **2014**, *293*, 299–305.
53. Xie, Y.; Hu, W.; Wang, X.; Tong, W.; Li, P.; Zhou, H.; Wang, Y.; Zhang, Y. Molten salt induced nitrogen-doped biochar nanosheets as highly efficient peroxymonosulfate catalyst for organic pollutant degradation. *Environ. Pollut.* **2020**, *260*, 114053.
54. Liu, X.; Zhangsun, G.; Zheng, Y.; Liang, S.; Cao, Y.; Liu, F.; Xiao, Y.; Jiang, L. Hierarchical N-doped carbons endowed with structural base sites toward highly selective adsorption and catalytic oxidation of H_2S. *Ind. Eng. Chem. Res.* **2021**, *60*, 2101–2111.
55. Rong, S.; Zhang, L.; Yue, Z.; Song, Z.; Tang, W.; Zhu, X.; Wang, T.; Zhou, X.; Cheng, S.; Xia, X. Directional introduction of pyridine nitrogen functional groups in activated carbon catalysts for the catalytic production of hydrogen: an experimental and DFT Calculation. *Chem. Eng. J.* **2023**, *453*, 139744.
56. Li, M.; Xu, F.; Li, H.; Wang, Y. Nitrogen-doped porous carbon materials: promising catalysts or catalyst supports for heterogeneous hydrogenation and oxidation. *Catal. Sci. Technol.* **2016**, *6*, 3670–3693.
57. Kundu, S.; Nagaiah, T.C.; Xia, W.; Wang, Y.; Dommele, S. Van; Bitter, J.H.; Santa, M.; Grundmeier, G.; Bron, M.; Schuhmann, W.; Muhler, M. Electrocatalytic activity and stability of nitrogen-containing carbon nanotubes in the oxygen reduction reaction. *J. Phys. Chem. C* **2009**, *113*, 14302–14310.
58. Li, O.L.; Chiba, S.; Wada, Y.; Panomsuwan, G.; Ishizaki, T. Synthesis of graphitic-N and amino-N in nitrogen-doped carbon via a solution plasma process and exploration of their synergic effect for advanced oxygen reduction reaction. *J. Mater. Chem. A* **2017**, *5*, 2073–2082.
59. Quílez-Bermejo, J.; Pérez-Rodríguez, S.; Canevesi, R.; Torres, D.; Morallón, E.; Cazorla-Amorós, D.; Celzard, A.; Fierro, V. Easy enrichment of graphitic nitrogen to prepare highly catalytic carbons for oxygen reduction reaction. *Carbon* **2022**, *196*, 708–717.
60. Quílez-Bermejo, J.; Pérez-Rodríguez, S.; Torres, D.; Canevesi, R.; Morallón, E.; Cazorla-Amorós, D.; Celzard, A.; Fierro, V. Nitrogen sites prevail over textural properties in N-doped carbons for the oxygen reduction reaction. *J. Colloid Interface Sci.* **2024**, *654*, 446–453.
61. Barrera, D.; Florent, M.; Sapag, K.; Bandosz, T.J. Insight into the mechanism of oxygen reduction reaction on micro/mesoporous carbons: ultramicropores versus nitrogen-containing catalytic centers in ordered pore structure. *ACS Appl. Energy Mater.* **2019**, *2*, 7412–7424. .
62. Wang, Y.; Zuo, S.; Liu, Y. Ammonia modification of high-surface-area activated carbons as metal-free electrocatalysts for oxygen reduction reaction. *Electrochim. Acta* **2018**, *263*, 465–473.
63. Wu, K.; Wang, D.; Su, D.; Gentle, I.R.A Discussion on the activity origin in metal-free nitrogen-doped carbons for oxygen reduction reaction and their mechanisms. *ChemSusChem* **2015**, *8*, 2772–2788.

 doi:10.20944/preprints202501.0451.v1

64. Wu, B.; Meng, H.; Morales, D.M.; Zeng, F.; Zhu, J.; Wang, B.; Risch, M.; Xu, Z.J.; Petit, T. Nitrogen-rich carbonaceous materials for advanced oxygen electrocatalysis: synthesis, characterization, and activity of nitrogen sites. *Adv. Funct. Mater.* **2022**, *32*, 2204137.
65. Li, S.; Xu, R.; Wang, H.; Brett, D.J.L.; Ji, S.; Pollet, B.G.; Wang, R. Ultra-high surface area and mesoporous N-doped carbon derived from sheep bones with high electrocatalytic performance toward the oxygen reduction reaction. *J. Solid State Electrochem.* **2017**, *21*, 2947–2954.
66. Zhang, Z.; Yu, L.; Tu, Y.; Chen, R.; Wu, L.; Zhu, J.; Deng, D. Unveiling the active site of metal-free nitrogen-doped carbon for electrocatalytic carbon dioxide reduction. *Cell Reports Phys. Sci.* **2020**, *1*, 100145.
67. Shang, Y.; Ding, Y.; Zhang, P.; Wang, M.; Jia, Y.; Xu, Y.; Li, Y.; Fan, K.; Sun, L. pyrrolic N or pyridinic N: the active center of N-doped carbon for CO2 reduction. *Chinese J. Catal.* **2022**, *43*, 2405–2413.
68. Li, C.; Wang, Y.; Xiao, N.; Li, H.; Ji, Y.; Guo, Z.; Liu, C.; Qiu, J. Nitrogen-doped porous carbon from coal for high efficiency CO_2 electrocatalytic reduction. *Carbon* **2019**, *151*, 46–52.
69. Sun, J.; Ge, Q.; Guo, L.; Yang, Z. Nitrogen doped carbon fibers derived from carbonization of electrospun polyacrylonitrile as efficient metal-free HER electrocatalyst. *Int. J. Hydrogen Energy* **2020**, *45*, 4035–4042.
70. Verma, J.; Goel, S. Cost-Effective Electrocatalysts for hydrogen evolution reactions (HER): challenges and prospects. *Int. J. Hydrogen Energy* **2022**, *47*, 38964–38982.
71. Cordero-Lanzac, T.; Rosas, J.M.; García-Mateos, F.J.; Ternero-Hidalgo, J.J.; Palomo, J.; Rodríguez-Mirasol, J.; Cordero, T. Role of different nitrogen functionalities on the electrochemical performance of activated carbons. *Carbon* **2018**, *126*, 65–76.
72. Fan, Y.; Yi, Z.; Zhou, Y.; Xie, L.; Sun, G.; Wang, Z.; Huang, X.; Su, F.; Chen, C. The relationship between the high-frequency performance of supercapacitors and the type of doped nitrogen in the carbon electrode. *New Carbon Mater.* **2024**, *39*, 1015–1026.
73. Yadav, A.; Kumar, R.; Joseph, D.; Thomas, N.; Yan, F.; Sahoo, B. Impact of dispersive solvent and temperature on supercapacitor performance of N-doped reduced graphene oxide. *C* **2024**, *10*, 89.
74. Hasegawa, G.; Deguchi, T.; Kanamori, K.; Kobayashi, Y.; Kageyama, H.; Abe, T.; Nakanishi, K. High-level doping of nitrogen, phosphorus, and sulfur into activated carbon monoliths and their electrochemical capacitances. *Chem. Mater.* **2015**, *27*, 4703–4712.
75. Zhai, Y.; Xu, B.; Zhu, Y.; Qing, R.; Peng, C.; Wang, T.; Li, C.; Zeng, G. Nitrogen-doped porous carbon from camellia oleifera shells with enhanced electrochemical performance. *Mater. Sci. Eng. C* **2016**, *61*, 449–456.
76. Zhang, Y.; Zhang, Y.; Huang, J.; Du, D.; Xing, W.; Yan, Z. Enhanced capacitive performance of N-doped activated carbon from petroleum coke by combining ammoxidation with KOH activation. *Nanoscale Res. Lett.* **2016**, *11*, 245.
77. Rashidi, N. A.; Yusup, S. Recent methodological trends in nitrogen–functionalized activated carbon production towards the gravimetric capacitance: a mini review. *J. Energy Storage* **2020**, *32*, 101757.
78. Han, W.; Wang, H.; Xia, K.; Chen, S.; Yan, P.; Deng, T.; Zhu, W. Superior nitrogen-doped activated carbon materials for water cleaning and energy storing prepared from renewable leather wastes. *Environ. Int.* **2020**, *142*, 105846.
79. Arango, D. I.; Zapata-Benabithe, Z.; Arenas, E. C.; Perez-Osorno, J. C. Influence of surface modification with nitric acid on electrochemical performance of agroindustrial waste-based activated carbon. *J. Mater. Sci. Mater. Electron.* **2018**, *29*, 15557–15569.
80. Shaker, M.; Ghazvini, A.A.S.; Shahalizade, T.; Gaho, M.A.; Mumtaz, A.; Javanmardi, S.; Riahifar, R.; Meng, X.; Jin, Z.; Ge, Q. A review of nitrogen-doped carbon materials for lithium-ion battery anodes. *New Carbon Mater.* **2023**, *38*, 247–278.
81. Yuan, R.; Hou, R.; Shang, L.; Liu, X.; Li, A.; Chen, X.; Song, H. The preparation and properties of N-doped carbon materials and their use for sodium storage. *New Carbon Mater.* **2024**, *39* (5), 770–795. .
82. Feng, S.; dos Santos, M.C.; Carvalho, B.R.; Lv, R.; Li, Q.; Fujisawa, K.; Elías, A.L.; Lei, Y.; Perea-López, N.; Endo, M.; Pan, M.; Pimenta, M.A.; Terrones, M. Ultrasensitive molecular sensor using N-doped graphene through enhanced raman scattering. *Sci. Adv.* **2016**, *2* (7).
83. Lawaniya, S.D.; Kumar, S.; Yu, Y.; Awasthi, K. Nitrogen-doped carbon nano-onions/polypyrrole nanocomposite based low-cost flexible sensor for room temperature ammonia detection. *Sci. Rep.* **2024**, *14*, 7904.

 doi:10.20944/preprints202501.0451.v1

84. Zhang, S.; Lan, D.; Zheng, J.; Kong, J.; Gu, J.; Feng, A.; Jia, Z.; Wu, G. Perspectives of nitrogen-doped carbons for electromagnetic wave absorption. *Carbon* **2024**, *221*, 118925.
85. Zhang, X.; Zhao, Z.; Xu, J.; Ouyang, Q.; Zhu, C.; Zhang, X.; Zhang, X.; Chen, Y. N-doped carbon nanotube arrays on reduced graphene oxide as multifunctional materials for energy devices and absorption of electromagnetic wave. *Carbon.* **2021**, *177*, 216–225.
86. Bianco, G.V.; Sacchetti, A.; Grande, M.; D'Orazio, A.; Milella, A.; Bruno, G. Effective Hole Conductivity in nitrogen-doped CVD-graphene by singlet oxygen treatment under photoactivation conditions. *Sci. Rep.* **2022**, *12*, 8703.
87. Ortega, K.F.; Arrigo, R.; Frank, B.; Schlögl, R.; Trunschke, A. Acid–base properties of N-doped carbon nanotubes: a combined temperature-programmed desorption, x-ray photoelectron spectroscopy, and 2-propanol reaction investigation. *Chem. Mater.* **2016**, *28*, 6826–6839.
88. Kundu, S.; Xia, W.; Busser, W.; Becker, M.; Schmidt, D.A.; Havenith, M.; Muhler, M. The formation of nitrogen-containing functional groups on carbon nanotube surfaces: a quantitative XPS and TPD study. *Phys. Chem. Chem. Phys.* **2010**, *12*, 4351.
89. Zhai, Y.; Pang, D.; Chen, H.; Xiang, B.; Chen, J.; Li, C.; Zeng, G.; Qiu, L. Effects of ammonization on the surface physico-chemical properties of sludge-based activated carbon. *Appl. Surf. Sci.* **2013**, *280*, 590–597.
90. Jansen, R.J.J.; van Bekkum, H. XPS of nitrogen-containing functional groups on activated carbon. *Carbon N. Y.* **1995**, *33* (8), 1021–1027.
91. Mainali, K.; Mood, S.H.; Pelaez-Samaniego, M.R.; Sierra-Jimenez, V.; Garcia-Perez, M. Production and applications of N-doped carbons from bioresources: a review. *Catal. Today* **2023**, *423*, 114248.
92. Newcombe, G.; Hayes, R.; Drikas, M. Granular activated carbon: importance of surface properties in the adsorption of naturally occurring organics. *Colloids Surfaces A Physicochem. Eng. Asp.* **1993**, *78*, 65–71.
93. Boehm, H. . Surface oxides on carbon and their analysis: a critical assessment. *Carbon N. Y.* **2002**, *40* (2), 145–149.
94. Ternero-Hidalgo, J.J.; Rosas, J.M.; Palomo, J.; Valero-Romero, M.J.; Rodríguez-Mirasol, J.; Cordero, T. Functionalization of activated carbons by HNO_3 treatment: influence of phosphorus surface groups. *Carbon N. Y.* **2016**, *101*, 409–419.
95. Puziy, A. M.; Poddubnaya, O. I.; Gawdzik, B.; Sobiesiak, M.; Sprynskyy, M. Structural evolution of polyimide-derived carbon during phosphoric acid activation. *C* **2022**, *8*, 47.
96. Elmouwahidi, A.; Bailón-García, E.; Pérez-Cadenas, A.F.; Maldonado-Hódar, F.J.; Carrasco-Marín, F. Activated carbons from KOH and H_3PO_4—activation of olive residues and its application as supercapacitor electrodes. *Electrochim. Acta* **2017**, *229*, 219–228.
97. Prauchner, M.J.; Rodríguez-Reinoso, F. Chemical versus physical activation of coconut shell: a comparative study. *Microporous Mesoporous Mater.* **2012**, *152*, 163–171.
98. Biesinger, M. C. Accessing the robustness of adventitious carbon for charge referencing (correction) purposes in XPS analysis: insights from a multi-user facility data review. *Appl. Surf. Sci.* **2022**, *597*, 153681.
99. Biesinger, M.C. X-ray Photoelectron Spectroscopy (XPS) Reference Pages—Label Oxygen. **Available online:** https://www.xpsfitting.com/search/label/Oxygen (Accessed on 22 dec 2024).
100. Beamson, G; Briggs, D. High resolution XPS of organic polymers: the Scienta ESCA300 Database. *J. Chem. Educ.* **1993**, *70*, A25.
101. Smith, M.; Scudiero, L.; Espinal, J.; McEwen, J.-S.; Garcia-Perez, M. Improving the deconvolution and interpretation of XPS spectra from chars by ab initio calculations. *Carbon.* **2016**, *110*, 155–171.
102. Herold, F.; Gläsel, J.; Etzold, B.J.M.; Rønning, M. Can temperature-programmed techniques provide the gold standard for carbon surface characterization? *Chem. Mater.* **2022**, *34*, 8490–8516.
103. Li, N.; Ma, X.; Zha, Q.; Kim, K.; Chen, Y.; Song, C. Maximizing the number of oxygen-containing functional groups on activated carbon by using ammonium persulfate and improving the temperature-programmed desorption characterization of carbon surface chemistry. *Carbon* **2011**, *49*, 5002–5013.
104. Razdyakonova, G.I.; Kokhanovskaya, O.A.; Likholobov, V.A. Influence of environmental conditions on carbon black oxidation by reactive oxygen intermediates. *Procedia Eng.* **2015**, *113*, 43–50.
105. Ishii, T.; Ozaki, J. Understanding the chemical structure of carbon edge sites by using deuterium-labeled temperature-programmed desorption technique. *Carbon.* **2020**, *161*, 343–349.

106. Vottero, E.; Carosso, M.; Pellegrini, R.; Piovano, A.; Groppo, E. Assessing the functional groups in activated carbons through a multi-technique approach. *Catal. Sci. Technol.* **2022**, *12*, 1271–1288.
107. Hall, P.J.; Calo, J.M. Secondary interactions upon thermal desorption of surface oxides from coal chars. *Energy & Fuels* **1989**, *3*, 370–376.
108. Düngen, P.; Schlögl, R.; Heumann, S. Non-linear thermogravimetric mass spectrometry of carbon materials providing direct speciation separation of oxygen functional groups. *Carbon N. Y.* **2018**, *130*, 614–622.
109. Göckeler, M.; Berger, C.M.; Purcel, M.; Bergsträßer, R.; Schinkel, A.-P.; Muhler, M. Surface reactions during temperature-programmed desorption and reduction experiments with oxygen-functionalized carbon blacks. *Appl. Surf. Sci.* **2021**, *561*, 150044.
110. Vivo-Vilches, J.F.; Bailón-García, E.; Pérez-Cadenas, A.F.; Carrasco-Marín, F.; Maldonado-Hódar, F.J. Tailoring the surface chemistry and porosity of activated carbons: evidence of reorganization and mobility of oxygenated surface groups. *Carbon* **2014**, *68*, 520–530.
111. Cândido, N.R.; Prauchner, M.J.; Vilela, A.D.O.; Pasa, V.M.D. The use of gases generated from eucalyptus carbonization as activating agent to produce activated carbon: An Integrated Process. *J. Environ. Chem. Eng.* **2020**, *8*, 103925.
112. Rodríguez-Reinoso, F.; Molina-Sabio, M. Textural and chemical characterization of microporous carbons. *Adv. Colloid Interface Sci.* **1998**, *76–77*, 271–294.
113. 113 Menendez, J.A.; Phillips, J.; Xia, B.; Radovic, L.R. On the modification and characterization of chemical surface properties of activated carbon: in the search of carbons with stable basic properties. *Langmuir* **1996**, *12*, 4404–4410.
114. Prauchner, M.J.; Sapag, K.; Rodríguez-Reinoso, F. Tailoring biomass-based activated carbon for CH_4 storage by combining chemical activation with H_3PO_4 or $ZnCl_2$ and physical activation with CO_2. *Carbon* **2016**, *110*, 138–147.
115. Prauchner, M.J.; Oliveira, S.D.C.; Rodríguez-Reinoso, F. Tailoring low-cost granular activated carbons intended for CO_2 adsorption. *Front. Chem.* **2020**, *8*, *581133*.
116. Pan, D.; Li, G.; Su, Y.; Wei, H.; Luo, Z. Kinetic study for the oxidation of cyclohexanol and cyclohexanone with nitric acid to adipic acid. *Chinese J. Chem. Eng.* **2021**, *29*, 183–189.
117. Soudani, N.; Souissi-najar, S.; Ouederni, A. Influence of nitric acid concentration on characteristics of olive stone based activated carbon. *Chinese J. Chem. Eng.* **2013**, *21*, 1425–1430.
118. Song, X.; Liu, H.; Cheng, L.; Qu, Y. Surface modification of coconut-based activated carbon by liquid-phase oxidation and its effects on lead ion adsorption. *Desalination* **2010**, *255*, 78–83.
119. Stöhr, B.; Boehm, H.P.; Schlögl, R. Enhancement of the catalytic activity of activated carbons in oxidation reactions by thermal treatment with ammonia or hydrogen cyanide and observation of a superoxide species as a possible intermediate. Carbon **1991**, *29*, 707-720.
120. Marchon, B.; Tysoe, W.T.; Carrazza, J.; Heinemann, H.; Somorjai, G.A. Reactive and kinetic properties of carbon monoxide and carbon dioxide on a graphite surface. *J. Phys. Chem.* **1988**, *92*, 5744–5749.